Journal of Archaeological Method and Theory (2027) 34:16
https://doi.org/10.1007/s10816-026-09828-7

RESEARCH

Characterizing Core Morphology and Scar Patterning Within a Unified Spherical Harmonic Framework

Pei-Yuan Xiao[1,2,3] · Hao Li[1,4] · Ben Marwick[3]

Received: 30 June 2026 / Accepted: 20 August 2026
© The Author(s), under exclusive licence to Springer Science+Business Media, LLC, part of Springer Nature 2026

Abstract
Lithic cores preserve the most direct evidence of past reduction strategies, yet their analysis still relies largely on typological classifications that are subjective and difficult to reproduce. Recent 3D methods quantify core attributes more precisely, but morphology and scar organization are handled in separate mathematical frameworks, precluding joint analysis of how the two relate. Here we present a unified framework based on spherical harmonics that encodes both core morphology (M-SPHARM) and scar patterning (SP-SPHARM) within a single rotation-invariant, landmark-free space, the latter being the first application of spherical harmonics to scar orientation data. Co-inertia analysis examines their covariation, and harmonic reconstruction renders statistical axes back into interpretable three-dimensional forms. While the methods are complementary, validation on ideal models and experimental cores shows that the scar pattern descriptor resolves finer distinctions among core types than existing metrics, most clearly the radial subtypes others cannot separate. The exploratory analysis on experimental and archaeological assemblages reveals no detectable covariation between morphology and scar organization. We identify core type as the principal factor structuring variation at Sandinggai (Hunan, China). The methods are released as an open-source R package (spharmlithic) with a fully reproducible workflow. More broadly, the framework supports understanding core variability as a continuous techno-morphological space rather than a set of discrete types.

Keywords Computational archaeology · Geometric morphometrics · Spherical harmonic · 3D lithic analysis · Core reduction strategy

Introduction

Cores accumulate the traces of flaking removals on their surface, and therefore record more of the knapping process than any individual flake. Their analysis can inform not only knapping behavior, including flaking strategies (Delagnes &

Extended author information available on the last page of the article

Published online: 02 September 2026

Meignen, 2006; Inizan & Féblot-Augustins, 1999; Pandey, 2025), reduction intensity (Clarkson, 2013; Lombao *et al.*, 2023a, 2023b), and knapping skill levels (Cattabriga & Peresani, 2024; Delpiano & Peresani, 2017; Eren *et al.*, 2011; Wilson *et al.*, 2023), but also broader questions of hominin cognition (H. Li *et al.*, 2017; Muller *et al.*, 2022), mobility patterns (Douglass *et al.*, 2018; Lombao *et al.*, 2023a, 2023b; Wallace & Shea, 2006), and social learning (Cattabriga *et al.*, 2024; Pargeter *et al.*, 2022; Valletta *et al.*, 2021). Core analysis has traditionally relied on typological approaches, in which cores are classified into categories such as Levallois, discoidal, and laminar cores according to hierarchically organized attributes such as morphology, scar patterning, flaking angles, and platform preparation (Boëda, 1993; Inizan & Féblot-Augustins, 1999). These frameworks, however, are often weakly standardized: different typological systems often employ distinct descriptive vocabularies, and substantial classification inconsistencies arise both between analysts and within the same analyst over time (Pargeter *et al.*, 2023; Ruck *et al.*, 2020; Whittaker *et al.*, 1998). The emerging debate over Levallois technology in China illustrates this problem clearly. Although researchers commonly apply the criteria proposed by Boëda (1995), disagreements persist over whether certain cores from the Shiyu and Guanyindong sites should be classified as Levallois (Carmignani *et al.*, 2024; Hu *et al.*, 2023; F. Li *et al.*, 2019; Yang *et al.*, 2024a, 2024b). Efforts to establish unified classificatory systems, such as the Unified Lithic Taxonomy and the Logic Analytical System, have partially reduced interobserver variability, yet they remain fundamentally reliant on qualitative judgment (Conard *et al.*, 2004; Lombao *et al.*, 2023a, 2023b).

Growing demands for precision and reproducibility have driven increasing interest in three-dimensional quantitative approaches to lithic analysis (Grosman *et al.*, 2008; Wyatt-Spratt, 2022). Three-dimensional modeling technologies provide substantially higher-resolution data than traditional linear measurements and have been widely applied to flakes (Archer *et al.*, 2021; Bustos-Pérez *et al.*, 2022), retouched tools (Falcucci & Peresani, 2022; Hashemi *et al.*, 2021), and large cutting tools (LCTs) (Herzlinger *et al.*, 2017; H. Li *et al.*, 2021). Studies specifically focused on cores, however, remain limited (Wyatt-Spratt, 2022). Three broad approaches characterize existing work. The first extracts predefined technological variables from 3D models, such as platform angles (Porter *et al.*, 2019), cortex proportions (Lin *et al.*, 2010), reduction intensity (Clarkson, 2013), surface convexity (Muller & Clarkson, 2026), and scar patterning (Clarkson *et al.*, 2006; Lin *et al.*, 2024). The second characterizes overall core morphology, most commonly through landmark-based geometric morphometrics (Hallinan & Cascalheira, 2025; Hallinan *et al.*, 2026; Lycett *et al.*, 2010), though recent studies have also applied spherical harmonic methods (SPHARM) to spheroids and polyhedral cores (Muller *et al.*, 2023; Ye *et al.*, 2026). These two approaches are complementary, and their integration has yielded deeper insights in several studies (Hallinan & Cascalheira, 2025; Hallinan *et al.*, 2026). A parallel line of work approaches core surfaces through mesh segmentation, in which individual scars are delineated on the 3D model and analyzed as graphs of adjacency and superposition (Linsel *et al.*, 2025; Liu *et al.*, 2026). This literature has developed largely independently of three-dimensional geometric morphometric research, but these approaches rest on the same underlying operation, performed manually or automatically: whether delineating a scar as a labeled region, placing landmarks along a core edge, or recording scar start and end points, each involves partitioning a three-dimensional surface, even where the analytical purposes differ.

Landmark-based approaches, however, have notable limitations. They compress continuous morphological variation into a limited number of discrete points, inevitably losing information (Bardua *et al.*, 2019; Goswami *et al.*, 2019; Gunz & Mitteroecker, 2013; Zelditch, 2004), although sliding semilandmarks recover much of this variation and improve correspondence across specimens (Bardua *et al.*, 2019; Gunz & Mitteroecker, 2013). They also rely on homology assumptions: current landmark configurations, which typically place landmarks along core edges and semi-landmarks across surfaces, are mainly applicable to highly standardized systems such as Levallois reduction and difficult to extend to more variable types or to cross-type comparisons (Hallinan & Cascalheira, 2025; Hallinan *et al.*, 2026; Lycett & Von Cramon-Taubadel, 2013; Lycett *et al.*, 2010). Even within Levallois core studies, landmark configurations vary between researchers, making direct comparisons between morphospaces problematic. Spherical harmonic approaches offer a promising alternative. They do not require homology assumptions, capture morphological information more comprehensively, and produce rotationally invariant power spectra that require no prior orientation of the core (Kazhdan *et al.*, 2003; Shen *et al.*, 2009). To date, however, their application has been largely restricted to near-spherical types such as spheroids and polyhedral cores (Muller *et al.*, 2023; Ye *et al.*, 2026), and their potential for more morphologically diverse core types has yet to be tested.

Quantitative approaches to scar pattern analysis are represented by two frameworks: the Scar Pattern Index (SPI), a univariate metric measuring directional concentration through the ratio of resultant to total vector length (Clarkson *et al.*, 2006), and fabric analysis, which uses eigenvalues of orientation tensors to provide a high-level summary of scar orientation (Lin *et al.*, 2024). Both represent important advances; yet both reduce complex scar-vector configurations to a small number of summary parameters that capture only relatively coarse-grained orientation organization rather than the full spatial structural properties of scar patterning itself. This information loss is reflected in their performance: SPI and fabric approaches effectively distinguish broad technological organizations, such as unidirectional or bidirectional removals and Levallois or discoidal cores (radial types), but struggle to differentiate variability within these categories. A method capable of representing the spatial structure of scar organization more completely, rather than reducing it to a few summary statistics, is therefore needed.

The relationship between the way scar organization documents how a core is reduced and the shape it ultimately assumes is an important question in lithic analysis. One influential body of theory holds that knappers actively structure removal sequences to generate and maintain particular core morphologies, most explicitly in prepared core types such as Levallois (Boëda, 1993, 1995; Brantingham & Kuhn, 2001). Other research theorizes that core form is also, and sometimes primarily, shaped by factors largely independent of technological intention, including raw material quality (Dibble, 1991; Kot *et al.*, 2020; Proffitt *et al.*, 2022; Terradillos-Bernal & Rodríguez-Álvarez, 2014), blank geometry (Proffitt *et al.*, 2022; Terradillos-Bernal & Rodríguez-Álvarez, 2014), and reduction intensity (Clarkson, 2013;

Lombao *et al.*, 2020). Whether, and to what degree, core morphology reflects deliberate technological design rather than the cumulative byproduct of working a given material therefore remains a genuinely open question, with direct bearing on how we infer planning, skill, and cultural transmission from stone tools. Distinguishing between these alternatives requires that technological organization and core morphology be quantified independently and that their covariation be tested directly, something no existing framework achieves within a single, reproducible representation. The problem is compounded by the available tools: scar pattern metrics such as SPI and fabric analysis compress organization into a handful of summary parameters, while landmark-based geometric morphometrics imposes homology assumptions that are tractable only for highly standardized forms and that differ from analyst to analyst. This constrains the cross-type, cross-assemblage, and cross-period comparison on which questions of technological origin and transmission ultimately depend.

Here we develop a spherical harmonic framework that represents core morphology and scar organization within a single mathematical space, recasting core variation from a set of discrete typological categories into a continuous, jointly quantified techno-morphological space. Scar vectors are converted into continuous spherical distributions through von Mises–Fisher kernel density estimation and expanded into rotation-invariant power spectra, placing scar organization in the same framework as morphology, which is described by the same expansion of the core surface. Because the method requires neither homologous landmarks nor manual orientation, its descriptors are directly comparable across core types, raw materials, regions, and time periods. Treating technology and morphology as separable but jointly analyzable dimensions, we use Co-inertia analysis to test their covariation and exploit the reconstructive capacity of spherical harmonics to translate statistical axes back into interpretable three-dimensional forms. We first validate the framework against digital models of idealized cores and an experimentally knapped set of cores. We then apply the framework in a case study using the core assemblage from Sandinggai, an open-air site with Late Pleistocene lithics in central South China. This application serves not as a regional end in itself, but as a worked example of a framework suitable for a variety of broader problems, from the contested status of Levallois in East Asia and the origins of prepared-core technologies to the reconstruction of technological transmission across hominin populations.

Materials and Methods

Materials

Three datasets were used in this study, each serving a distinct analytical role. The idealized digital cores dataset was used to evaluate the sensitivity of spherical harmonic methods to standardized scar patterns. The experimentally knapped cores dataset was employed to test the scar pattern analysis framework under more realistic conditions of morphological and technological variability and evaluate the integrated statistical framework proposed in this study. The archaeological specimens dataset was then analyzed within this validated framework to demonstrate its practical archaeological applicability.

Idealized Digital Cores

Eight idealized digital core models, sourced from Lin *et al.* (2024), were used, comprising cylindrical, conical, discoidal (unifacial and bifacial), Levallois (preferential, convergent, and laminar), biface, and polyhedral types. Each category is associated with distinct and highly recognizable scar organizations, which can be visually examined in the interactive HTML files provided as Online Resource 2.

Experimentally Knapped Cores

The experimental cores were produced by Chris Clarkson and comprise 58 specimens used in this study: 16 unidirectional, 6 bidirectional, 21 Levallois (10 preferential, 5 convergent, 2 Nubian, 2 recurrent, and 2 laminar), 5 discoidal, and 10 multiplatform cores. These specimens are curated at the School of Social Sciences, University of Queensland. The cores were digitized by Sam Lin using a Polyga HDI Compact C210 structured-light scanner with FlexiScan3D software (Lin *et al.*, 2024).

Archaeological Specimens

The archaeological specimens derive from Sandinggai (hereafter SDG) in Hunan Province, China, previously reported by H. Li *et al.* (2022). The SDG sequence comprises three cultural layers (L2, L3, and L4), dated by optically stimulated luminescence (OSL) to approximately 100–20 ka. The lithic assemblage is characterized by two operational sequences: (1) a small-flake system primarily based on chert, and (2) a large-flake and LCT system primarily based on quartz sandstone (H. Li *et al.*, 2022).

From the previously reported SDG core assemblage, 51 complete and well-preserved specimens retaining clear technological information were selected for analysis, after excluding incomplete, heavily abraded, and test cores. These derive from Layers 2, 3, and 4; however, because only two cores originate from Layer 2, our statistical analyses were restricted to Layers 3 and 4. Core classifications follow the original paper, and details of core types and raw materials are provided in Table 1. Archaeological cores were digitized using an EinScan Pro 3D scanner (SHINING 3D) operated in fixed-scan mode with a turntable and fixed camera stand (single-shot accuracy 0.05 mm; point distance 0.16 mm). Model alignment and export were completed using the accompanying EinScan-Pro software.

For both experimental and archaeological datasets, postprocessing was conducted in Geomagic Wrap 2021, including the filling of minor holes and the correction of mesh defects such as non-manifold edges and self-intersections.

Table 1 Specimen inventory of the analyzed Sandinggai (SDG) core assemblage, listed by core type, raw material, and stratigraphic layer

Core type	Chert	Sandstone	Layer 3	Layer 4	Total
Unifacial unidirectional	7	0	4	3	7
Unifacial centripetal	12	0	5	7	12
Bifacial adjacent	4	4	4	4	8
Bifacial independent	3	0	1	2	3
Bifacial centripetal	1	0	0	1	1
Multifacial	6	7	3	10	13
Core on flake	4	1	1	4	5
Total	37	12	18	31	49

Counts include the analyzed cores from Layers 3 and 4; the two Layer 2 cores were excluded from the statistical analyses because of their insufficient sample size. Core type classifications follow the original study

Data Extraction

Scar orientations were recorded following the protocol established by Lin *et al.* (2024). Each scar was recorded as a vector defined by the three-dimensional coordinates of its start and end points, using Geomagic Wrap 2021 for data acquisition. All visually identifiable scars were annotated without a size limit; a minimum-size criterion was then applied at the data-processing stage, excluding scars whose direction vector was shorter than 2 mm. Because this criterion is applied to the complete record rather than during annotation, the threshold can be varied without re-annotating the material, which is what makes the scar size sensitivity analysis reported below possible. Note that the vector length is measured along the direction of removal and is not necessarily the maximum extent of the scar. A best-fit plane was also calculated for each core model, and the coordinates of the plane centroid and a normal vector were exported for model alignment.

Two alignment procedures were employed to eliminate initial phase differences among core models. Both operate on the scar vector data; the morphological descriptor is aligned separately by centroid normalization and principal-axis alignment (see "Spherical Harmonic Analysis" section). The first follows Lin *et al.* (2024), aligning models based on their best-fit planes by rotating the plane normal to coincide with the Z-axis and translating the starting point of the longest scar to the global origin. The second procedure is proposed here for the first time and relies exclusively on the spatial organization of scar data. Singular value decomposition (SVD) factorizes the $n \times 3$ matrix of scar unit vectors into orthogonal directions ranked by the amount of variance each accounts for: the first singular vector captures the dominant direction of scar organization, while the third captures the direction along which scar orientations vary least—that is, the normal to the plane in which the scars are most nearly contained. The procedure is as follows: (1) unit vectors are calculated for all scars and subjected to SVD; (2) the third singular vector is selected as the alignment-plane normal and rotated to the Z-axis; (3) the global centroid of all scar coordinates is translated to the origin; and (4) the first singular vector is aligned with the X-axis.

The original vectors and the vectors aligned under both procedures were then used to evaluate the rotational invariance of the scar pattern metrics described below. To allow direct visual inspection of the alignment outcomes, interactive HTML visualizations of each model under both procedures are provided as Online Resource 2.

Spherical Harmonic Analysis

Spherical harmonic analysis represents the three-dimensional extension of elliptic Fourier analysis (Harper *et al.*, 2022; Shen *et al.*, 2009). The method characterizes surfaces of closed genus-zero objects by mapping each vertex onto the unit sphere through equivalent coordinate functions and representing the surface as a weighted sum of spherical harmonic basis functions (Brechbühler *et al.*, 1995; Shen *et al.*, 2009). The resulting shape descriptors are invariant to rotation, translation, and scaling, and can be used to reconstruct the original three-dimensional morphology directly (Kazhdan *et al.*, 2003). SPHARM was originally developed for morphometric analysis of brain structures in medical imaging and has since been applied across multiple disciplines (Gerig *et al.*, 2001; Medyukhina *et al.*, 2020; Radvilaitė *et al.*, 2016). In lithic studies, Sholts *et al.* (2017) used spherical harmonics to quantify asymmetry in Clovis points, while Muller *et al.* (2023) and Ye *et al.* (2026) applied the method to spheroid morphology. Beyond morphological characterization, mathematical relationships between spherical harmonic representations and directional data have also been established (Lee *et al.*, 2022). In the present study, we exploit this relationship by applying SPHARM to scar orientation data for the first time, as shown in Fig. 1.

Our analytical workflow for scar pattern analysis proceeds as follows. Discrete scar vectors are first transformed into a continuous density distribution on the sphere using von Mises–Fisher spherical kernel density estimation (vMF-sKDE) (Alonso-Pena *et al.*, 2024; Bai *et al.*, 1988):

$$f(\mathbf{g}) = \frac{1}{n}\sum_{i=1}^{n} \exp\left(\kappa\, \mathbf{g} \cdot \mathbf{x}_i\right)$$

where $\boldsymbol{g}$ is a unit vector on the spherical grid, $\boldsymbol{x}_i$ is the unit vector representing the orientation of the i-th scar, and $\boldsymbol{\kappa}$ is the concentration parameter of the von Mises–Fisher kernel, related to the bandwidth $\boldsymbol{h}$ by:

$$\kappa = \frac{1}{h^2}$$

A bandwidth of 0.35 ($\boldsymbol{\kappa} \approx 8.16$) was selected to balance directional resolution against oversmoothing. This choice was validated by reconstructing the original distributions, in which distinct scar patterns remained clearly identifiable.

The KDE distributions were interpolated onto a 64×128 Driscoll–Healy grid and subjected to spherical harmonic expansion. Each distribution $f(\theta, \phi)$ is represented as a weighted combination of spherical harmonic basis functions $Y_l^m(\theta, \phi)$:

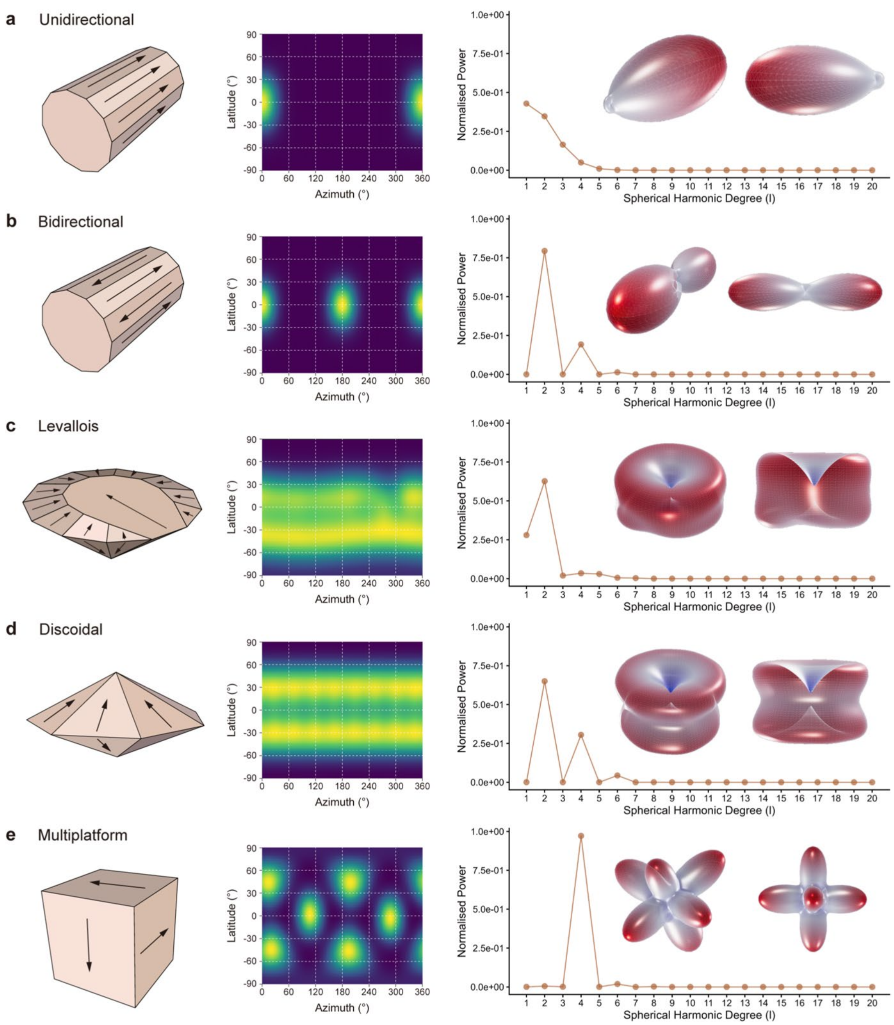

Fig. 1 Application of spherical harmonic analysis to scar orientation data, demonstrated on five idealized core types: **a** unidirectional, **b** bidirectional, **c** Levallois, **d** discoidal, and **e** multiplatform. For each type, the idealized 3D core model and its scar pattern are shown on the left, converted into a continuous spherical density using a von Mises–Fisher kernel density estimation in the middle, and represented by a rotation-invariant power spectrum. The scar pattern reconstructed from the harmonic coefficients is shown on the right

$$f(\theta,\phi)=\sum_{l=0}^{\infty}\sum_{m=-l}^{l}\widehat{f}(l,m)\,Y_l^m(\theta,\phi)$$

where the coefficients $\widehat{f}(l,m)$ quantify the contribution of each basis function, and $\boldsymbol{l}$ and $\boldsymbol{m}$ denote harmonic degree and order, respectively. A truncation threshold of $l_{\max}$ = 20 was adopted in our study, consistent with previous studies demonstrating that this degree sufficiently captures detailed artifact morphological variation (Ye *et al.*, 2026). The resulting coefficients retain phase information and can be used to reconstruct original three-dimensional forms, but phase sensitivity may introduce noise in comparative analyses. Accordingly, scar pattern spherical harmonic (hereafter SP-SPHARM) power spectra were also calculated by summing squared coefficients within each harmonic degree and normalizing to unit total, providing a phase-independent, rotationally invariant representation of scar pattern structure.

Terminology in this area is not fully settled. We follow Clarkson *et al.* (2006), whose Scar Pattern Index provides one of our comparative baselines, in using "scar pattern" for the spatial and directional organization of scar orientations on a core; the same usage appears in Bretzke and Conard (2012), Lombao *et al.* (2023a, 2023b), Lombao *et al.* (2024) and Cao *et al.* (2025); Lin *et al.* (2024) employ "scar organization" and "scar patterning" interchangeably. The term is also used, however, for diacritic analysis, which reconstructs the relative order of removals from inter-scar ridge morphology (Kot *et al.*, 2025; Linsel *et al.*, 2025). These address different dimensions of the same evidence, and we use "scar pattern" throughout in the former sense only: SP-SPHARM encodes where and in which direction removals were struck, and carries no information about the order in which they occurred.

For core morphological analysis, we followed the procedures established by Ye *et al.* (2026). Three-dimensional models (.stl) were downsampled to 20,000 faces, and Laplacian smoothing was applied to reduce surface noise and regularize vertex distribution. Centroid normalization and principal-axis alignment were then performed to position all vertices within a common coordinate system, which was transformed into spherical coordinates for harmonic expansion. Spherical harmonic coefficients and morphological spherical harmonic (hereafter M-SPHARM) power spectra were calculated at $l_{\max} = 20$, as for the scar pattern analysis. The complete workflow is illustrated in Fig. 2.

Although coefficients were computed to $l_{\max} = 20$ for faithful reconstruction, retaining all 20 degrees for statistical comparison would add dimensionality and, for scar patterns, noise. We therefore screened degrees prior to all statistical analyses using two diagnostics that bound the choice from opposite directions: cumulative power, indexing the share of total variance each degree carries (a lower bound on the degree needed), and the across-specimen coefficient of variation (CV), indexing the reliability of each degree's between-specimen signal (an upper bound beyond which degrees are noise-dominated). The two spectra behaved differently and were truncated on different grounds. For SP-SPHARM, cumulative power was effectively exhausted by the fifth to sixth degree, while higher degrees were noise-dominated (CV > 100% from $\boldsymbol{l} \approx 9$). The two diagnostics therefore delimit an acceptable interval rather than a single value; within that interval we retained $\boldsymbol{l} = 1$–6, the lowest-dimensional setting for which the results remain stable (Online Resource 1: Table S5). For M-SPHARM, between-specimen signal remained reliable across all degrees (CV < 90% throughout), but variance was strongly concentrated in the low degrees, with ~98% of cumulative power captured by the eighth degree; we retained $\boldsymbol{l} = 1$–8, since the reliable but very low-energy higher degrees (together under 2% of power) would inflate dimensionality and dilute multivariate comparisons without materially improving discrimination. This contrast confirms that scar pattern spectra are markedly lower-dimensional than morphological spectra (Fig. 3).

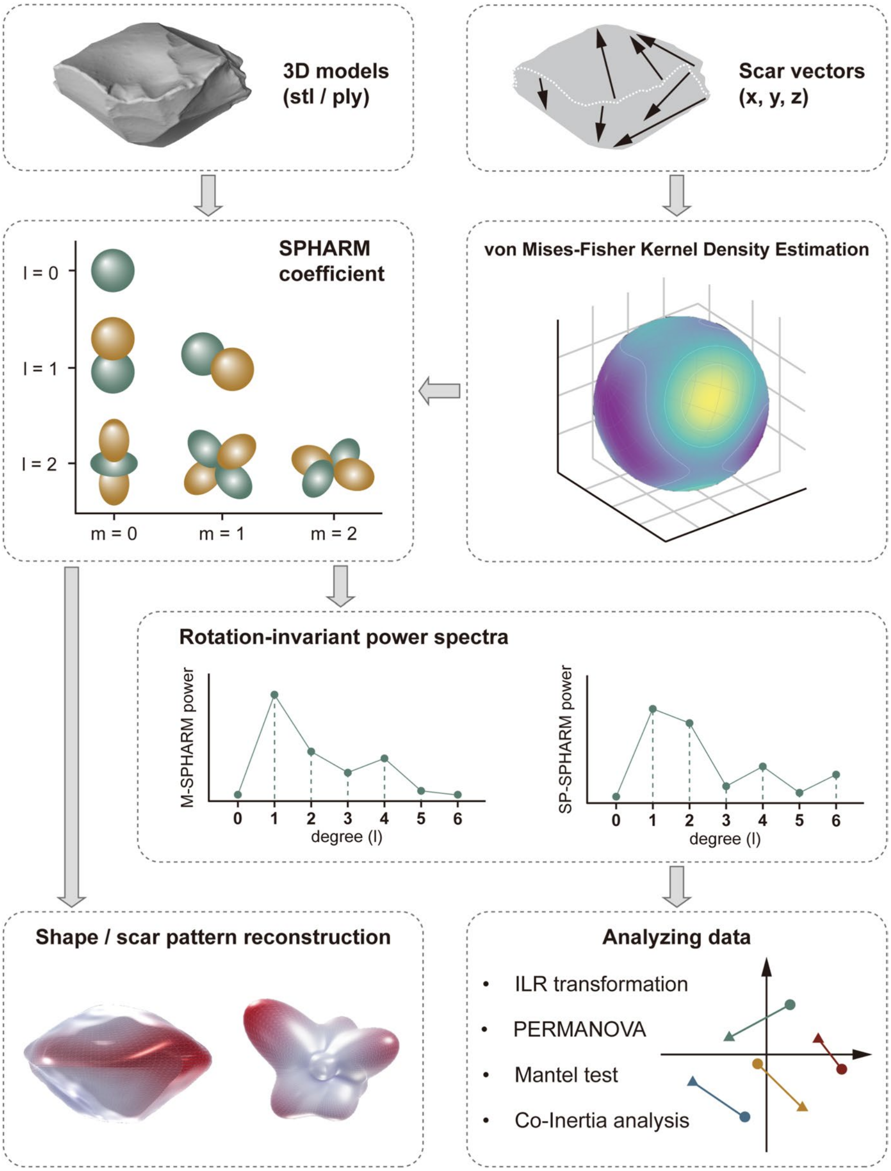

Fig. 2 Overview of the unified spherical harmonic workflow for jointly describing core morphology and scar organization

Data Analysis

Rotation Invariance Assessment

Comparing specimens with these metrics presupposes that each captures the scar pattern itself rather than the arbitrary orientation in which a model happens to

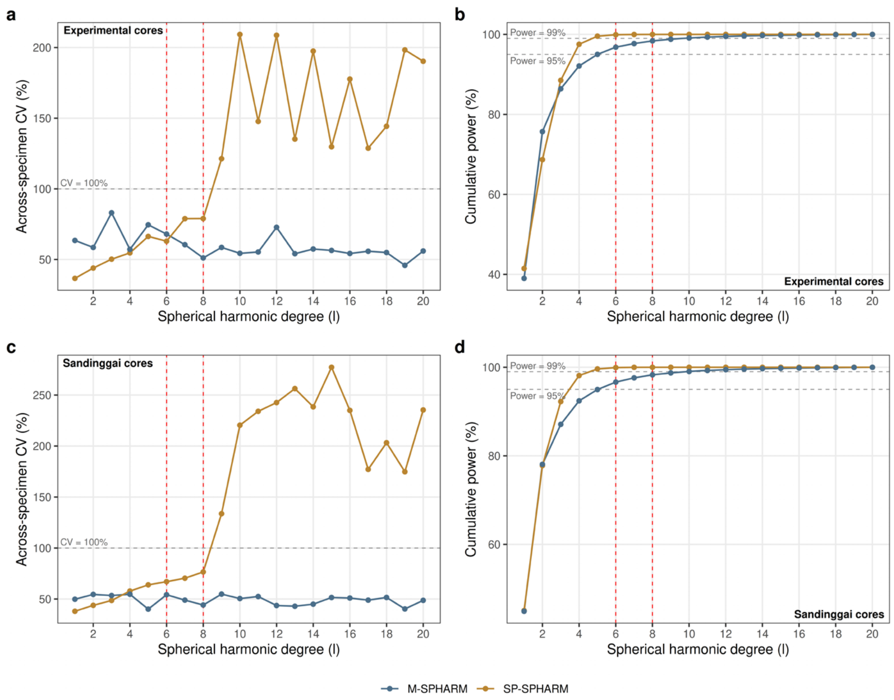

Fig. 3 Per-degree diagnostics used to select the spherical harmonic truncation degree, shown for the experimentally knapped cores and the Sandinggai assemblage. **a** and **c** Across-specimen coefficient of variation (CV) by harmonic degree l and **b** and **d** cumulative power by harmonic degree l. In each panel, the morphology (M-SPHARM) and scar pattern (SP-SPHARM) power spectra are overlaid. Dashed lines mark the 100% CV reference in **a** and **c** and the 95% and 99% cumulative power references in **b** and **d**

be digitized. We therefore first evaluated whether each metric is independent of model orientation, that is, whether its value is stable across the original orientation and the two alignment procedures described above. Rotational invariance of three scar pattern metrics (SPI, fabric Elongation and Isotropy, and SP-SPHARM power spectra) was assessed using the Bland–Altman approach. This method evaluates agreement between paired measurements by plotting their difference against their mean (Bland & Altman, 1986, 1999). The mean difference represents systematic bias, and the 95% limits of agreement (LoA) define the range within which 95% of differences are expected to fall; narrow LoA with no systematic trends indicate high agreement (Bland & Altman, 1999). Each metric was computed under three coordinate conditions: (1) original scar-vector data, (2) morphological-plane alignment, and (3) technological-plane alignment. Pairwise Bland–Altman comparisons among these conditions were conducted, with high agreement interpreted as evidence of rotational invariance.

Method Comparison

For the idealized digital cores, where only one model exists per type, discriminatory power was assessed using pairwise distances in feature space, with greater distances indicating stronger inter-type separation; because the SP-SPHARM power spectra are compositional, we used standardized Euclidean distances on Isometric log-ratio transformation (ILR) coordinates (Aitchison, 1982), whereas SPI and fabric used standardized Euclidean distances on the raw features. Results were visualized using heatmaps. For the experimentally knapped cores, a significance-testing framework was employed. SPI, as a univariate metric, was evaluated using the Kruskal–Wallis test (Kruskal & Wallis, 1952). Fabric metrics and SP-SPHARM descriptors were analyzed using PERMANOVA, which tests overall structural differences between groups, complemented by PERMDISP to assess whether differences in within-group dispersion contribute to the observed separation (Anderson, 2001, 2006). Significant PERMDISP results warrant cautious interpretation of PERMANOVA outcomes (Anderson, 2006, 2017). All permutation procedures used 9999 permutations. Where overall tests were significant, *post hoc* pairwise comparisons were performed with Holm–Bonferroni correction (Holm, 1979).

Techno-morphological Statistical Analytical Framework

To investigate technomorphology relationships, we employed a two-step analytical framework: first testing whether overall covariation exists between M-SPHARM and SP-SPHARM power spectra using Mantel and RV tests, then exploring interaction patterns through joint dimensional reduction using Co-inertia analysis. All comparisons in this section are between these two descriptor blocks, scar pattern and morphology, computed for the same specimens. The experimental and archaeological assemblages are analyzed separately and are never compared to one another.

Isometric Log-Ratio Transformation ILR transformation is a preparatory step rather than a test: it removes a constraint inherent to power spectra so that all subsequent analyses operate in Euclidean space. It carries no archaeological reading of its own, but is the precondition for the steps that follow. Spherical harmonic power spectra are compositional data: the total power is constrained to a fixed sum, so variation in one harmonic degree necessarily induces spurious covariance among others (Aitchison, 1982; Greenacre, 2021). To eliminate this closure constraint, ILR was applied to all power spectrum data, projecting them into Euclidean space through log-ratio calculations among harmonic degrees (Egozcue *et al.*, 2003). All subsequent statistical analyses were conducted on ILR-transformed data. For the comparison analyses in which SP-SPHARM is placed alongside the non-compositional SPI and fabric metrics, the ILR coordinates were additionally standardized so that distances are expressed on a common scale across methods.

Mantel Test and RV Coefficient Overall covariation was evaluated using two complementary approaches. The Mantel test and the RV coefficient ask whether scar patterns and morphology covary at all, from two complementary angles. The Mantel test compares pairwise distance structures, asking whether cores that resemble one another in overall form also resemble one another in scar organization. The RV coefficient compares multivariate covariance structures, asking instead how much of the variation in the two dimensions is shared. The Mantel test assesses a correlation between two distance matrices via Spearman's rank correlation coefficient, with significance determined by 9999 permutations (Mantel, 1967). The RV coefficient quantifies the overall degree of association between two multivariate datasets, ranging from 0 (no association) to 1 (identical structure), with significance likewise assessed by permutation (Escoufier, 1973; Robert & Escoufier, 1976). The Mantel test emphasizes pairwise distance relationships, whereas the RV coefficient focuses on multivariate covariance structure; their combined use therefore provides a more robust assessment of dataset correspondence.

Co-Inertia Analysis Co-inertia analysis (CoIA) is a multivariate method for evaluating structural relationships between two datasets. Co-inertia analysis is used here descriptively rather than as a test: it extracts the axes of maximal shared variation between the two blocks, identifying which aspects of core form correspond to which aspects of scar organization, so that the relationship, whether or not it is statistically supported, can be described and visualized for each specimen individually. Its core principle is to identify directions of variation along which the two datasets are maximally concordant while maximizing their covariance (Dolédec & Chessel, 1994; Dray *et al.*, 2003). PCA is first performed separately on each dataset, after which projections are used to identify correspondences among samples and variables across the two data spaces (Dolédec & Chessel, 1994; Dray *et al.*, 2003). CoIA is particularly well suited for comparing datasets that differ in physical meaning but share identical sampling units, making it especially appropriate for jointly analyzing M-SPHARM and SP-SPHARM power spectra, which describe different aspects of core variability across the same set of specimens.

The CoIA ordination axes represent the principal directions of shared variation between the two datasets. Each sample, in our case each core, is represented by two points, one from the M-SPHARM analysis, and one from the SP-SPHARM analysis, connected by a line segment. Line length reflects the degree of discrepancy between a sample's position in the two data spaces: shorter lines indicate stronger correspondence between its morphological and scar pattern signatures, whereas longer lines indicate that the two dimensions characterize that specimen differently (Dolédec & Chessel, 1994; Dray *et al.*, 2003). Line direction reflects the trend of covariation for that sample within the shared space. If line directions are broadly consistent across a group of samples, this suggests a stable and internally coherent covariation structure. Dispersed directions suggest weaker structural correspondence or the presence of localized variation. Combined with the reconstructive capacity of spherical harmonics, this framework allows the morphological and scar pattern characteristics associated with each end of the CoIA axes to be directly visualized as three-dimensional forms, thereby reconnecting statistical patterns to concrete archaeological interpretation.

To further characterize sample correspondences, we employed Kruskal–Wallis tests to compare line lengths among groups, assessing whether the degree of technology–morphology coupling differs across core types (Kruskal & Wallis, 1952). Rayleigh tests were applied to line directions to evaluate whether orientations exhibit significant directional clustering (Mardia, 1988). Because line directions in CoIA represent axial correspondences rather than unidirectional vectors, they were treated as axial data, with directions differing by 180° considered equivalent (Arnold & SenGupta, 2006; Mark, 1973). The combined analysis of line lengths and directions enables a simultaneous evaluation of coupling strength and structural consistency from both distance-based and directional perspectives. The whole workflow is shown in Fig. 4.

Reconstruction Along CoIA Axes To visualize the coupled techno-morphological variation captured by CoIA, we developed a continuous reconstruction framework operating directly in spherical harmonic coefficient space. Spherical harmonic coefficients of individual specimens were projected onto the CoIA axes, and at evenly spaced positions along each axis, reconstructed forms were generated by Gaussian kernel-weighted averaging of neighboring specimens' coefficients (Hutton *et al.*, 2003). The weighted coefficients were then transformed back into three-dimensional meshes (M-SPHARM) or spherical density surfaces (SP-SPHARM) through inverse spherical harmonic reconstruction. The resulting forms represent localized structural tendencies along covariance gradients rather than static group averages, enabling gradual transitions in morphology and scar organization to be visualized as continuous trajectories within the shared CoIA space.

Joint Discriminant Analysis To assess the discriminatory power of the two descriptors in combination, rather than their covariation, the ILR-transformed M-SPHARM and SP-SPHARM coordinates were merged into a single feature space following the block normalization convention of Multiple Factor Analysis (MFA): each centered block is divided by its own first singular value, so that no block dominates the joint space through scale alone. PERMANOVA and the associated pairwise comparisons were then computed on the full Euclidean distance matrix of the merged coordinates, retaining all axes; because the global PCA of the merged block is an orthogonal rotation, distances are unchanged when all axes are kept, so the joint model is directly comparable to the two single-block models.

The relative contribution of the two blocks is a free parameter, so we also varied it directly. Each block was rescaled so that morphology accounted for a fixed share w of the total squared distance, and the analysis was repeated as w was increased from 0 (scar patterning only) to 1 (morphology only). This makes w directly interpretable as the weight given to morphology relative to scar patterning. Results are reported both as the number of Holm-corrected pairwise separations and as the median $-\log_{10}$-transformed value of the uncorrected pairwise *p*-values. Because a *p*-value provides a measure of the incompatibility of the observed data with the

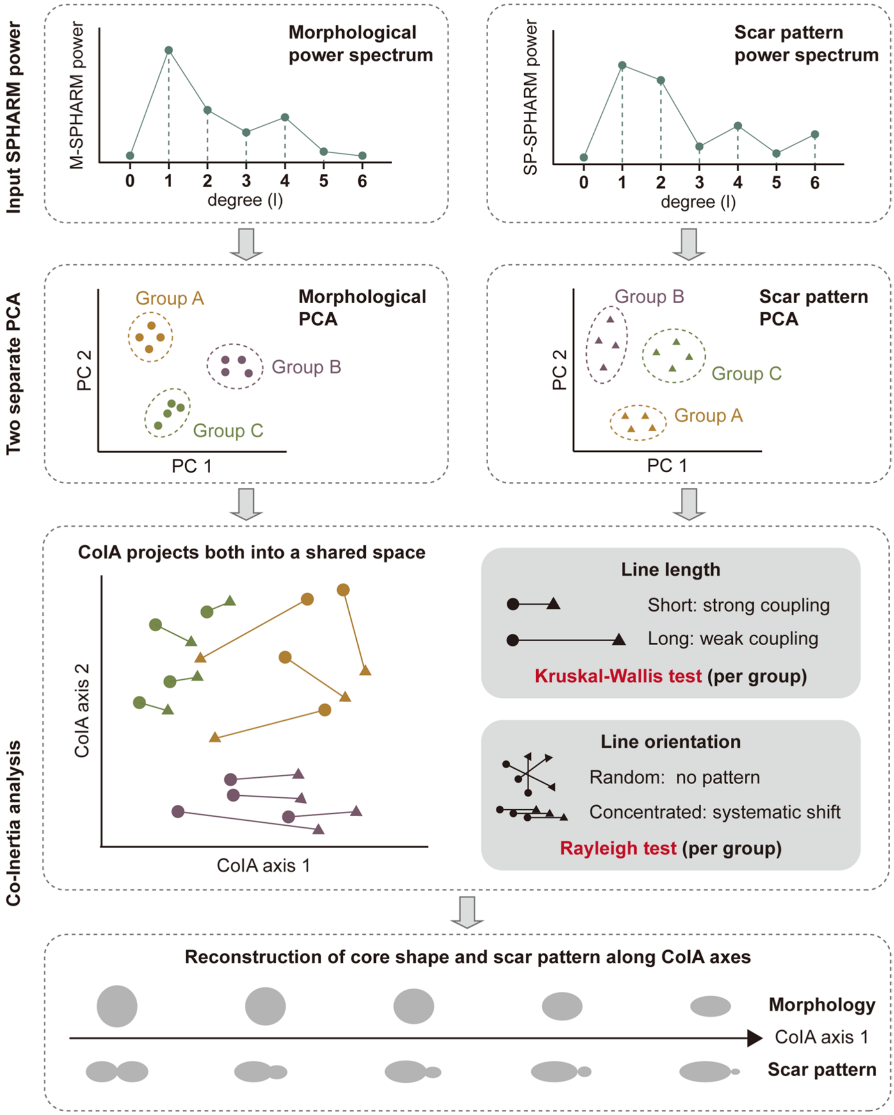

Fig. 4 Workflow of the Co-inertia analysis (CoIA) framework. The two inputs are the M-SPHARM and SP-SPHARM power spectra of the same set of cores; the analysis is run separately for the experimental and the archaeological assemblage

null model rather than supporting a binary decision (Wasserstein & Lazar, 2016), expressing the uncorrected *p*-values on a continuous scale captures variation that a thresholded count cannot: a pair whose *p*-value falls from 0.04 to 0.004 contributes nothing additional to the count, but its $-\log_{10}$-transformed value increases from 1.40 to 2.40.

Reduction Intensity To test whether core variation at SDG is structured by how far each core had been reduced, we used the scar density index (SDI) as a continuous proxy for core reduction intensity (Clarkson, 2013). SDI was entered as a continuous term in PERMANOVA models of each descriptor block, following raw material and core type in sequential sums of squares, so that it is assessed as an increment over the categorical factors already considered. Raw material × SDI and layer × SDI interactions were tested in the same way, to establish whether any absence of a main effect could arise from opposing trends between groups.

Sensitivity Analysis Because the proposed descriptors involve several analyst-defined computational parameters, sensitivity analysis provides a necessary check on whether the reported patterns reflect an empirical structure in the data rather than idiosyncratic parameter choices (Hamby, 1994; Saltelli, 2002). To confirm that our conclusions do not depend on specific parameter choices, we conducted parameter sensitivity analysis varying the four principal free parameters of the two descriptors: the von Mises–Fisher kernel bandwidth and the minimum scar size threshold for SP-SPHARM, and the mesh decimation target and number of Laplacian smoothing iterations for M-SPHARM. Full procedures and complete results are reported in Online Resource 1; the outcomes relevant to each analysis are noted in the Results and Discussion below.

Power Analysis To evaluate whether non-significant association results could be attributed to a limited sample size, we assessed the range of covariation that the present sample design could reasonably detect. Rather than calculating observed power from the realized effect, which is not informative for interpreting a completed test (Hoenig & Heisey, 2001), we evaluated what size of association the present sample design could reasonably detect (Lakens, 2022). To do this, we combined three checks: a bias-corrected RV coefficient, bootstrap estimates of the plausible upper range of the association, and simulations testing whether Mantel and RV tests would detect known levels of covariation at the realized sample sizes (Rohlf & Corti, 2000). The procedure and full results are reported in Online Resource 1.

Reproducibility and Open-Source Materials

Computational reproducibility remains an ongoing challenge in archaeological science, yet it is essential for the credibility and cumulative progress of quantitative research (Marwick, 2017; Marwick *et al.*, 2017). To support reproducibility and reuse, all materials necessary to reproduce the analyses presented here are provided in a version-controlled online repository at OSF (https://doi.org/10.17605/OSF.IO/D82C5). Three-dimensional models are archived in both .stl and .ply formats. The .ply files are numerically exact re-encodings of the .stl used in the analyses, verified for all specimens (identical face counts, face-index arrays and vertex coordinates); the analysis pipeline takes .stl as input, so retaining both formats allows the reported results to be reproduced exactly while providing the .ply format preferred for downstream computational work. These materials include the complete R and Python scripts used for all analyses and visualizations, and the raw datasets underlying all reported results. The repository is organized following established best practices for research compendia, with a folder structure and relative file paths that allow all code to be executed without manual modification. All figures, tables, and statistical results presented in this paper can therefore be independently reproduced from these materials.

In addition, we provide an open-source R package (spharmlithic) that implements the essential analytical methods developed in this study, including model alignment, SPI and fabric computation, spherical harmonic analysis of both scar patterns and core morphology, and three-dimensional visual reconstruction (Xiao & Marwick, 2026). This package is designed as a general-purpose tool to enable other researchers to apply these methods to their own datasets.

Results

Validity Analysis

Rotational Invariance of Scar Pattern Analysis Measures

SPI and fabric metrics showed near-perfect agreement across all three coordinate conditions (original, morphological-plane aligned, and technological-plane aligned), with biases and 95% LoA on the degree of 10^{-16}, well within floating-point numerical precision (Goldberg, 1991; Higham, 2002). Both measures are therefore effectively rotationally invariant, and coordinate alignment is not required prior to their computation (Fig. 5).

SP-SPHARM descriptors exhibited small systematic biases in low-degree power ($l = 1 - 2$; 95% $LoA = \pm 0.02$), which diminished rapidly with increasing degree; no substantive differences were observed for $l \geq 3$ (Fig. 5). Random rotational perturbations around the Z-axis produced differences within machine precision, confirming that directional uncertainty within the coordinate frame has no effect on the power spectrum given a fixed Z-axis.

The low-degree biases most likely originate from upstream computational steps such as KDE interpolation and coordinate mapping rather than from the power spectrum formulation itself. Crucially, a consistent alignment method applied uniformly across all specimens ensures that this systematic error does not alter relative differences among them. All subsequent analyses therefore employ the technological fitted plane for alignment.

Validity of the SPHARM Method for Scar Pattern Analysis

Test of Idealized Models Inter-type separation increased progressively from SPI to fabric metrics to SP-SPHARM descriptors, as revealed by the pairwise distance heatmaps (Fig. 6). Mean distances confirmed this ordering: SP-SPHARM yielded

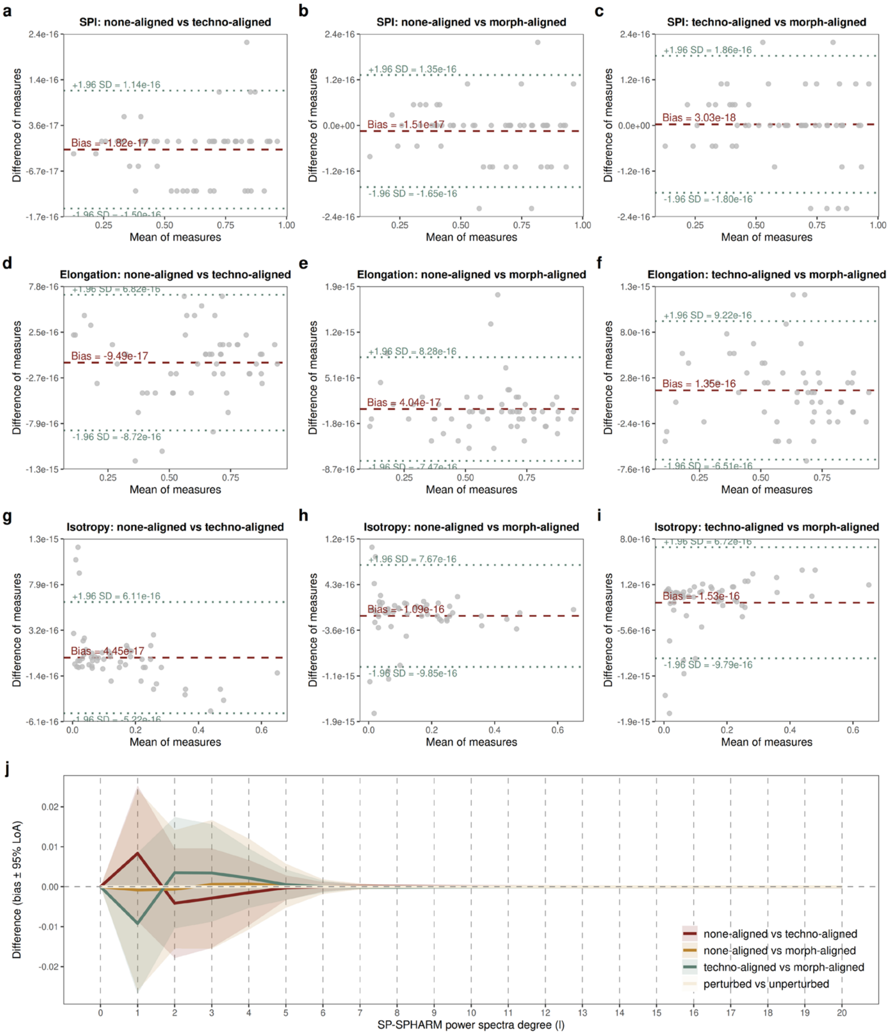

Fig. 5 Bland–Altman analysis of rotational invariance. **a–c** SPI across three coordinate conditions. **d–f** Fabric elongation ratio across three coordinate conditions. **g–i** Fabric isotropy ratio across three coordinate conditions. **j** SP-SPHARM power spectra bias across three coordinate conditions and random Z-axis perturbation

the greatest overall separation ($\overline{d}_{\mathrm{E,std}} = 1.94$), exceeding fabric metrics ($\overline{d}_{\mathrm{E,std}} = 1.66$) and SPI ($\overline{d}_{\mathrm{E,std}} = 1.12$).

SPI produced moderate distances between unidirectional types (cylindrical, conical) and radial or centripetal types (discoidal, Levallois), but near-zero distances among Levallois subtypes (preferential, convergent, and laminar) and between discoidal variants, indicating that it primarily captures the degree of directional concentration while remaining insensitive to finer structural differences. Fabric metrics substantially improved separation between unidirectional and radial categories but,

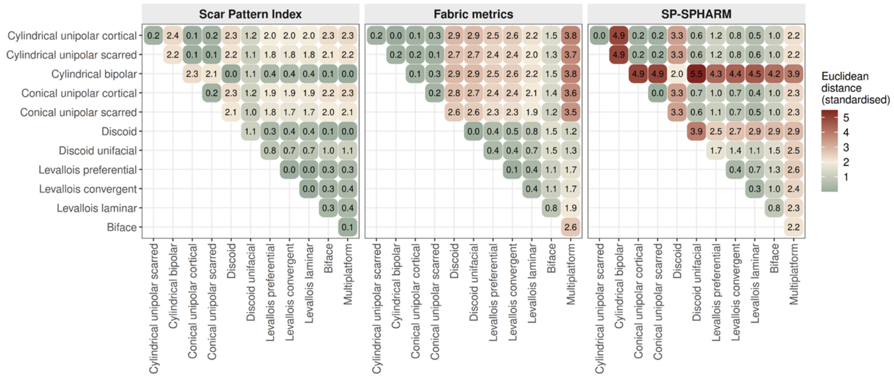

Fig. 6 Discriminatory power of the three scar pattern analytical methods on the idealized digital cores, shown as heatmaps of pairwise standardized distances between core types for SPI, fabric metrics, and SP-SPHARM power spectra. For SP-SPHARM, the distances are standardized Euclidean distances on ILR coordinates; for SPI and fabric, they are standardized Euclidean distances on the raw features. Larger distances indicate stronger separation

like SPI, failed to distinguish scar patterns sharing parallel but opposing orientations. Distances between unipolar and bipolar cylindrical types remained near zero. SP-SPHARM produced the highest pairwise distances across nearly all comparisons. Notably, it achieved clear separation between discoidal and Levallois types and between bifacial and unifacial discoidal patterns, distinctions that neither SPI nor fabric metrics resolved. Multiplatform cores were most strongly differentiated from all other types under SP-SPHARM. However, distances between types sharing bipolar symmetry in the power spectrum domain, such as bifacial discoidal and bipolar cylindrical patterns, remained comparatively modest, foreshadowing a limitation also observed in the experimentally knapped core analysis below.

Test of Experimentally Knapped Cores To evaluate the sensitivity of each method on empirical data, we computed all three measures for experimentally knapped cores and conducted statistical comparisons by core type. All three methods detected significant inter-type differences (Fig. 7), but they resolved different sets of distinctions. SP-SPHARM descriptors separated the broadest set of type pairs, including several that neither summary metric could. Fabric metrics distinguished the majority of type pairs but failed to differentiate unidirectional from bidirectional cores. SPI was the most limited, detecting differences only where unidirectional cores were involved.

These results suggest that the three methods are complementary. SP-SPHARM descriptors capture the overall structure of scar patterning for most pairwise comparisons, though separation is reduced for patterns with bipolar symmetry, such as discoidal–bidirectional pairs (p_{adj} = 0.392). Fabric metrics effectively distinguishes differences between unidirectional and bidirectional cores from Levallois and discoidal cores, but cannot differentiate unidirectional from bidirectional cores (p_{adj} = 0.072), nor Levallois from discoidal cores (p_{adj} = 0.055). SPI is most sensitive to the unidirectional type but shows limited discriminative capacity for other types. Notably, although SP-SPHARM descriptors failed to separate discoidal from

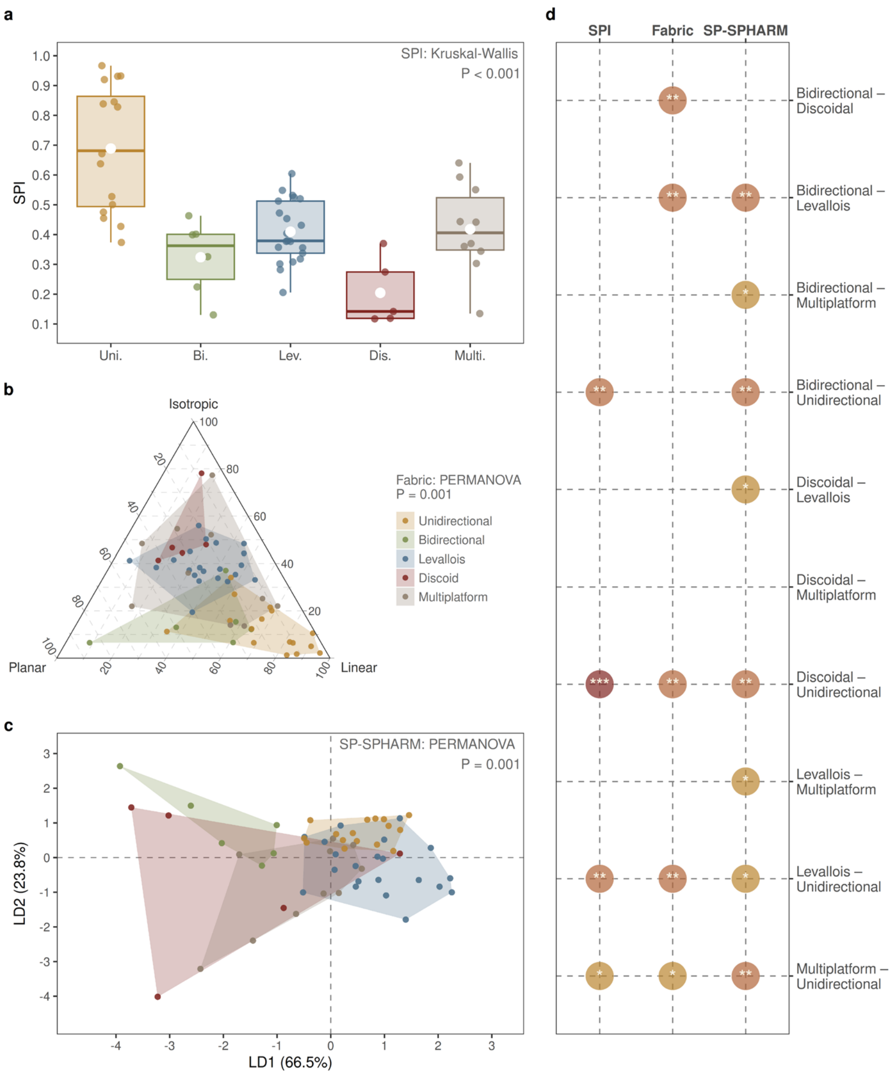

Fig. 7 Comparison of the three scar pattern analytical methods on the experimentally knapped cores, grouped by core type: **a** Box-and-whisker plot of SPI distributions by core type with a Kruskal–Wallis testing result; **b** fabric metrics shown as a Benn ternary diagram of elongation, planar, and isotropy components with a PERMANOVA result; and **c** SP-SPHARM descriptors

bidirectional cores due to their similarity structures in SPHARM power spectrum (Fig. 6), this distinction is successfully recovered by fabric metrics ($p_{adj} = 0.01$). PERMDISP on the SP-SPHARM descriptors was significant ($p = 0.002$), driven mainly by the greater within-group dispersion of discoidal (and, more weakly, Levallois) cores relative to unidirectional cores. We therefore interpret the PERMANOVA cautiously, noting that the two non-significant pairs (discoidal–bidirectional and discoidal–multiplatform) both involve the discoidal group, which combines high dispersion with a small sample ($n=5$).

To confirm that this type discrimination was not driven disproportionately by small, less reliably recorded scars, we repeated the analysis with scars at or below 5 mm and then 10 mm progressively excluded. The overall PERMANOVA by core type remained significant at every threshold (R^2 = 0.282–0.322, all $p < 0.05$), and pairwise resolution varied only marginally, separating eight of ten pairs at the > 2 mm baseline, seven at > 5 mm and nine at > 10 mm (Online Resource 1: Table S2). The core type signal was therefore carried primarily by the larger, more reliably recorded removals and was robust to excluding the smallest scars. A complementary test perturbed the recorded scar vectors themselves. Discrimination was insensitive to angular error, but sensitive to polarity error: reversing 10% of vectors reduced pairwise resolution from eight to five of ten pairs. Fabric metrics were, by construction, unaffected by polarity reversal, indicating that SP-SPHARM retains directional information that is not captured by orientation-tensor summaries, as discussed below (Online Resource 1: Table S3, Fig. S5).

Joint Analysis of Scar Patterns and Core Morphology in Experimental Knapping Specimens

Combining morphology and scar patterning, PERMANOVA recovered a significant overall difference by core type (R^2 = 0.211, pseudo-F = 3.553, p = 0.0001; Fig. 8). *Post hoc* pairwise comparisons resolved the same number of type pairs, and the same specific pairs, as SP-SPHARM alone (8 of 10). The distribution of pairwise resolution across different weight values was unchanged across the entire range in which morphology contributed no more than half of the squared distance ($w \leq 0.5$). However, the median $-\log_{10}(p)$ across all pairs was higher than at the scar pattern-only setting throughout the 0 to 0.5 weight range, rising from 2.84 at $w = 0$ to a maximum of 3.19 at $w = 0.25$. This indicates that combining the two descriptors improved the strength of the evidence rather than the number of separable pairs; at weight values greater than 0.5 discrimination declined progressively. The standard MFA normalization falls within this stable interval. We note that the optimal weighting depends on the relative information content of the two descriptors in a given assemblage, and is therefore specific to the present assemblage and typology rather than generalizable.

PERMANOVA tests using M-SPHARM descriptors showed core type to account for a small but statistically significant fraction of morphological variation (R^2 = 0.123, pseudo-F = 1.864, p = 0.025), with no individual type pair resolved after Holm–Bonferroni correction. Despite this weak structuring of morphology by core type, the global Mantel test likewise revealed no significant correlation between M-SPHARM and SP-SPHARM descriptor sets (Mantel's $r = -0.061$, p = 0.796), and the RV coefficient from CoIA did not reach significance (RV = 0.101, p = 0.12). Both association measures were negligible in magnitude, indicating that core morphology and scar organization vary largely independently at the assemblage level.

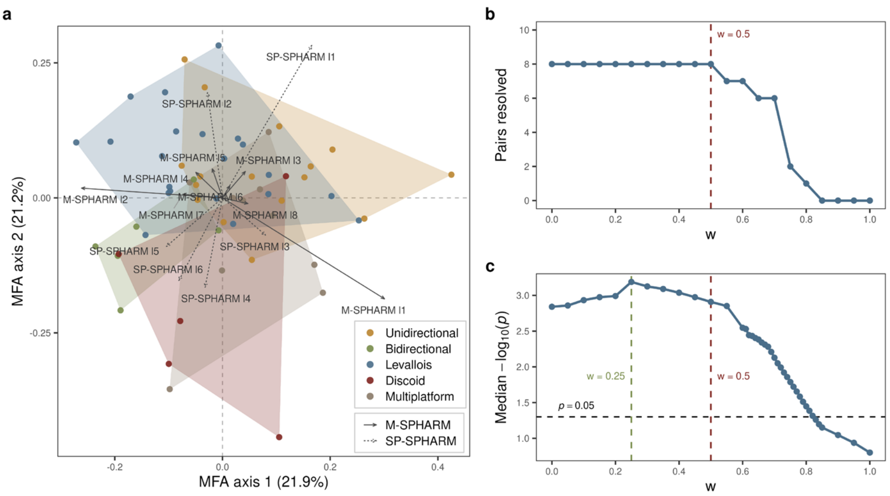

Fig. 8 Joint discriminant analysis of M-SPHARM and SP-SPHARM descriptors for the experimentally knapped cores, after Multiple Factor Analysis (MFA) block normalization. **a** MFA biplot on the first two axes; each core is a point colored by core type, with convex hulls per type, and the descriptor loadings shown as arrows (solid, M-SPHARM; dashed, SP-SPHARM, labeled by spherical harmonic degree). **b** The number of core type pairs resolved after Holm–Bonferroni correction as a function of the morphology weight w, the share of the total squared distance contributed by morphology. **c** Median $-log_{10}(p)$ across all ten pairs as a function of w. In **b** and **c**, the dark red dashed line marks equal weighting ($w =$ 0.50), the position at which the standard MFA normalization falls; in **c**, the olive dashed line marks the maximum of the median curve, and the black dashed horizontal line marks $-log_{10}(0.05) = 1.30$

Because the global tests above provide no evidence of covariation, the CoIA axes are interpreted here descriptively, as the directions of maximal shared variation extracted by the method, rather than as a statistically supported covariance structure. The first two CoIA axes account for 85.6% of total covariation (Axis 1 = 65.5%, Axis 2 = 20.1%; Fig. 9). Along Axis 1, M-SPHARM reconstructions shift from rounded, equidimensional forms to progressively flattened profiles, while SP-SPHARM reconstructions transition from concentrated, directionally organized density distributions to more dispersed, multidirectional patterns characteristic of centripetal or multiplatform scar organizations. Axis 2 captures a secondary morphological gradient from laterally convex, disk-shaped cross-sections to more uniform, flattened elliptical forms. On the scar pattern side, both axes capture broadly similar transitions in scar organization, reflecting a shift from ordered, directionally structured arrangements, such as unidirectional and bidirectional patterns, toward more dispersed, multidirectional configurations typical of discoidal and multiplatform cores (Fig. 9).

Kruskal–Wallis tests revealed no significant difference in line lengths across core types (Fig. 9), indicating that the degree of morphology–scar correspondence does not differ detectably across reduction strategies. Overall, the experimental assemblage shows no detectable covariation between core morphology and scar pattern: both the global Mantel test and the RV coefficient are negligible. At the within-type level, no core type showed significant directional clustering of CoIA line directions (all Rayleigh $p > 0.05$). This broader pattern suggests that morphology and

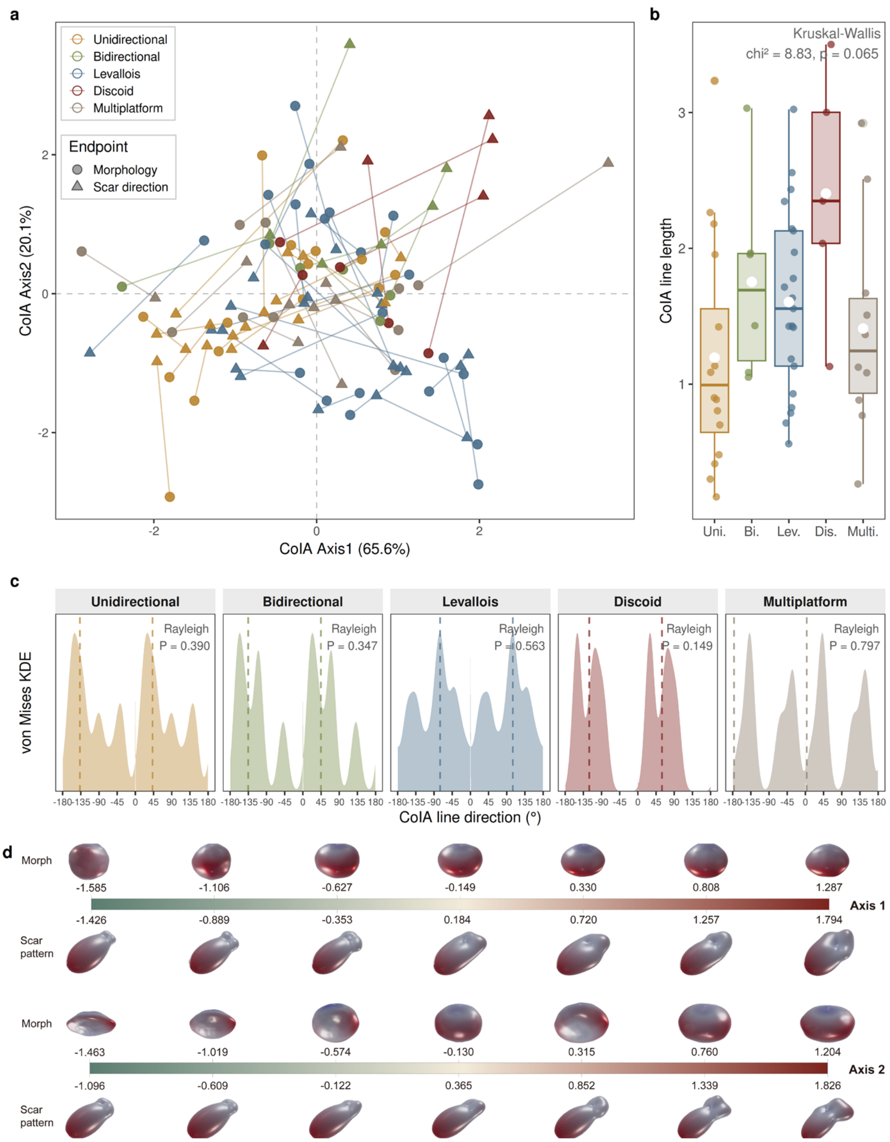

Fig. 9 Co-inertia analysis (CoIA) of M-SPHARM and SP-SPHARM descriptors for the experimentally knapped cores. **a** CoIA ordination on the first two axes; each core is shown as a morphology point (circle) and a scar pattern point (triangle) joined by a line, whose length and direction summarize the morphology–scar pattern correspondence for that specimen. **b** Line lengths compared among core types using Kruskal–Wallis test. **c** Rose diagrams of line directions by core type with Rayleigh testing results. **d** Morphology (top) and scar pattern (bottom) reconstructed along the CoIA axes by inverse spherical harmonic reconstruction

scar organization vary primarily along relatively independent axes; under the current sample conditions, no statistically meaningful techno-morphological coupling trajectory can be detected.

Case Study: Core Analysis from Sandinggai

As with the experimental cores, the global Mantel test revealed no significant correlation between M-SPHARM and SP-SPHARM descriptors for the SDG assemblage (Mantel's $r = 0.012$, $p = 0.427$). Cross-frequency Mantel tests remained non-significant after Holm–Bonferroni correction, confirming that no covariation is detectable in any frequency band. The RV coefficient likewise did not reach significance ($RV = 0.091$, $p = 0.313$).

As in the experimental assemblage, the non-significant global tests mean that the CoIA axes below are read descriptively rather than as evidence of a real covariance structure. The first two CoIA axes account for 90.6% of total covariation (Axis 1 = 57.6%, Axis 2 = 33.0%; Fig. 10). Along Axis 1, M-SPHARM reconstructions transition from flattened, dorsoventrally compressed forms to more rounded, equidimensional profiles, while SP-SPHARM reconstructions shift from concentrated, unidirectionally organized density distributions to more symmetrically opposed, bidirectional patterns. Axis 2 captures additional variation in both dimensions. On the scar pattern side, it distinguishes unidirectional and bidirectional organizations from more centripetal, dispersed configurations. On the morphology side, it primarily reflects mid-frequency shape variation associated with three-fold and four-fold rotational symmetry, likely corresponding to differences in core cross-sectional geometry (Fig. 10).

Line lengths showed no significant differences among layers ($\chi^2 = 0.17$, df = 1, $p = 0.678$), raw materials ($\chi^2 = 0.57$, df = 1, $p = 0.45$), or core types ($\chi^2 = 10.2$, df = 5, $p = 0.07$; Fig. 10), indicating that the degree of morphology–scar correspondence does not differ detectably across any grouping condition. Rayleigh tests on line direction revealed no significant directional concentration in any layer, raw material, or core type (all $p > 0.05$). The absence of any directionally structured group indicates that the decoupling between morphology and scar organization holds consistently down to the within-type level, with no core type showing a structured techno-morphological trajectory.

PERMANOVA identified core type as the dominant factor structuring both dimensions, with significant and comparable effects on morphological and scar pattern variation, whereas raw material and layer each accounted for substantially less variation (Table 2). Raw material explained only a small, non-significant fraction of morphological variation and had a negligible effect on scar pattern, while layer effects were negligible for both dimensions, consistent with continuity in knapping behavior across the stratigraphic sequence.

Two patterns emerge from these effect sizes. First, core type explained roughly four to five times more variation than either raw material or layer in both dimensions, identifying it as the principal axis of structured variability at SDG. Second, although core type significantly structured both morphology and scar organization, the two dimensions showed no detectable pairwise covariation (Mantel's $r = 0.012$;

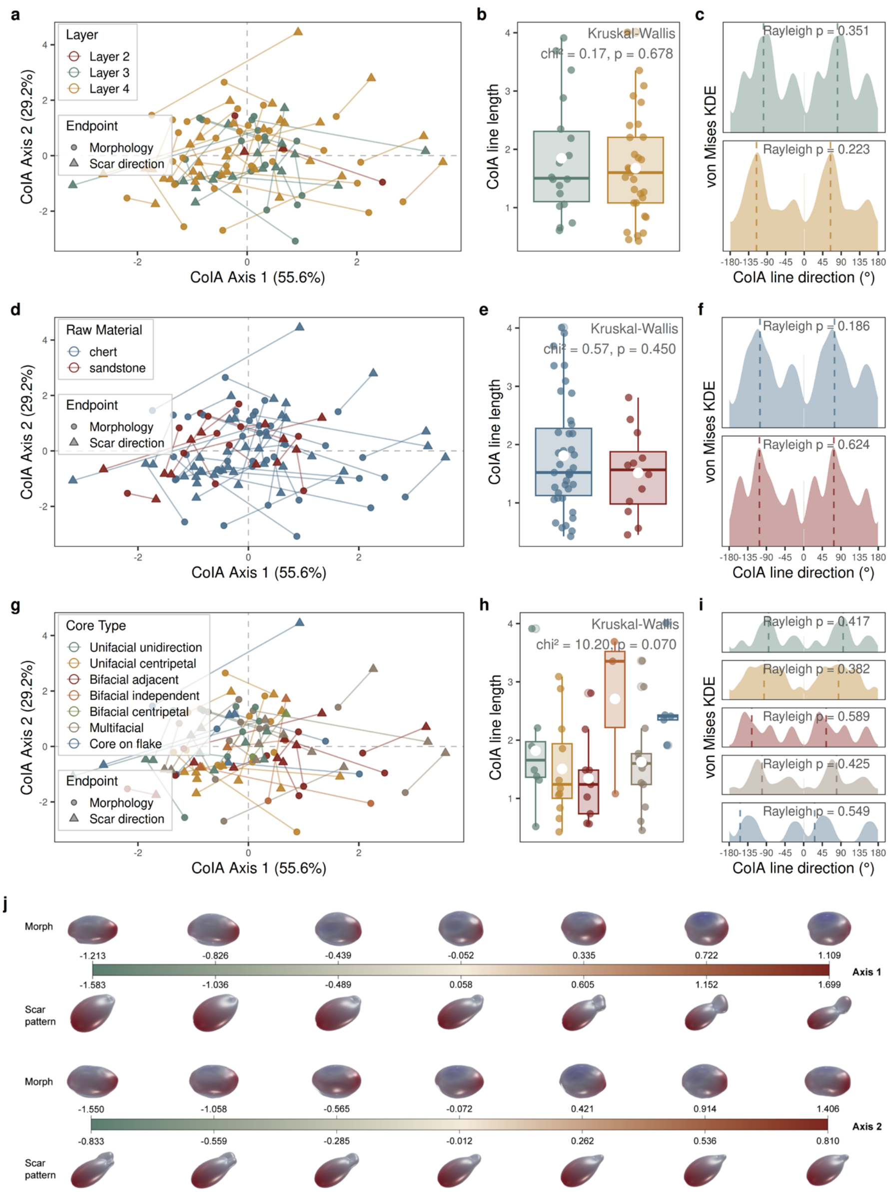

Fig. 10 Co-inertia analysis (CoIA) of M-SPHARM and SP-SPHARM descriptors for the Sandinggai core assemblage, with specimens grouped by stratigraphic layer **a**–**c**, raw material **d**–**f**, and core type **g**–**i**. In each grouping, the CoIA ordination (left) shows every core as a morphology point (circle) and a scar pattern point (triangle) joined by a line; the center panel compares line lengths among groups (Kruskal–Wallis test) and the right panel shows rose diagrams of line directions (Rayleigh test). **j** Morphology (top) and scar pattern (bottom) reconstructed along the CoIA axes by inverse spherical harmonic reconstruction

Table 2 PERMANOVA results for the Sandinggai core assemblage, Layers 3 and 4 only

Term	df	M-R^2	M-pseudo-F	M-p	SP-R^2	SP-pseudo-F	SP-p
Core type	5	0.188	2.030	0.010	0.168	1.780	0.040
Raw material	1	0.041	2.080	0.080	0.018	0.905	0.435
Layer	1	0.018	0.842	0.491	0.020	0.948	0.415

Each variable (core type, raw material, and layer) was tested in a separate PERMANOVA using 9999 permutations, for both the morphology (M-SPHARM) and scar pattern (SP-SPHARM) descriptors. R^2, proportion of variance explained; pseudo-F, PERMANOVA test statistic; p, permutation-based p-value

RV = 0.091): type-level differences in form and in scar organization are not aligned along a shared axis, each responding to core type but largely independently of the other. The somewhat larger effect of raw material on morphology ($R^2 = 0.041$) than on scar organization ($R^2 = 0.018$) is consistent with material properties influencing form more than reduction organization, but both effects are small and this tendency should not be overinterpreted at the present sample size.

The three factors considered so far are categorical. Because the framework also yields continuous descriptors, we additionally tested whether reduction intensity, measured as the SDI, structures either dimension. It did not: once raw material and core type were accounted for, SDI explained little variation in scar pattern, morphology, and both together ($R^2 = 0.017$–0.027, all $p > 0.18$). Raw material × SDI and layer × SDI interactions were likewise non-significant, indicating that this null result does not arise from opposing trends between raw materials or between layers.

Discussion

The principal contribution of this study is conceptual as much as methodological. By embedding scar organization and core morphology within a single rotation-invariant, landmark-free mathematical framework, it treats lithic core variability as a continuous techno-morphological space rather than a collection of discrete types. This framework enables scar patterning and form to be quantified separately and their relationship assessed directly. In this section, we first evaluate the robustness of the approach across diverse reduction systems, then examine what the decoupling of scar organization and morphology reveals about knapping behavior, and finally we consider its implications for long-standing cross-regional questions. By providing a homology-free, period-agnostic descriptor of core variation, our framework offers analytical possibilities beyond those available to conventional landmark-based approaches.

The validity of SP-SPHARM for characterizing scar organization is supported statistically: PERMANOVA confirms that it discriminates most scar-pattern categories. Reconstructions of the idealized models, experimentally knapped cores, and SDG specimens render these differences in an interpretable form. Because they are generated from the same manually recorded vectors, these reconstructions illustrate rather than independently verify the result. A reasonable concern is whether this discrimination is driven disproportionately by small, less reliably recorded scars.

As reported in our validity analysis above, it is not. The non-significant distinction between discoidal and multiplatform cores is particularly informative. It reflects the high internal variability of the multiplatform category, within which certain specimens exhibit scar patterns resembling those of discoidal cores. Importantly, this overlap does not imply that these specimens should be reclassified (Lin *et al.*, 2024). Rather, it shows that scar organization does not map one-to-one onto conventional typological categories but encodes a technological variation that those categories—which bundle morphology and scar pattern into a single label—cannot isolate. This reinforces the value of quantifying scar organization as a dimension of core variability distinct from, and complementary to, morphology.

Compared with existing quantitative approaches to scar pattern analysis, SP-SPHARM demonstrates clear advantages, although it does not constitute a complete replacement for either the SPI or the fabric method. SPI is fundamentally a measure of directional concentration. It quantifies the degree to which scar orientations converge toward a single resultant direction and is therefore most sensitive to unidirectional patterns, while performing poorly in discriminating among radial or centripetal scar organizations (Clarkson *et al.*, 2006). The fabric method adds a second analytical dimension by characterizing variation in orientations perpendicular to the best-fit core plane, thereby enabling separation between bidirectional and radial core types that SPI cannot achieve (Lin *et al.*, 2024). However, because fabric metrics are derived from orientation-tensor eigenvalues, they summarize axial orientation structure rather than vector polarity. In the eigenvalue method for axial data, reversing the sense of an observation does not change the orientation matrix (Mark, 1973), while fabric-shape indices such as elongation and isotropy describe whether orientations form linear, planar, or isotropic configurations (Benn, 1994; McPherron, 2018). Consequently, geometrically parallel scar patterns that differ mainly in technological polarity, such as unidirectional and bidirectional arrangements, may produce similar fabric configurations, as also suggested by Lin *et al.* (2024). In contrast, SP-SPHARM encodes the spatial structure of scar organization more completely, rather than compressing it into summary parameters. This is what allows it to separate radial subtypes such as Levallois and discoidal cores, a distinction that neither SPI nor fabric metrics achieve. However, SP-SPHARM reconstructions represent continuous density distributions that cannot be straightforwardly mapped onto discrete scar pattern categories. By contrast, SPI and fabric indices retain stronger direct physical interpretability. In practice, an effective workflow is to first assess overall group differences using SP-SPHARM, and then integrate SPI and fabric analyses to refine an archaeological interpretation.

At the level of practical implementation, the three methods also differ in their sensitivity to coordinate alignment. SPI and fabric metrics are strictly rotationally invariant, requiring no alignment prior to computation. SP-SPHARM power spectra show small systematic biases in low-degree terms attributable to upstream computational steps, necessitating a consistent alignment procedure across all specimens (Fig. 5). This additional requirement is a practical cost, but one that is offset by the finer structural distinctions SP-SPHARM resolves. More broadly, all three quantitative approaches share an important advantage over traditional scar pattern classification: they replace subjective categorical judgments with continuous numerical descriptors, thereby reducing interobserver inconsistency and enabling reproducible, statistically testable comparisons across assemblages.

The lack of systematic covariation between core morphology and scar patterning is not unexpected because the same core morphology can be produced through more than one organization of removals: blade and Levallois production both admit unipolar and bipolar configurations. Our framework adds the ability to test this expectation rather than assume it by integrating M-SPHARM and SP-SPHARM power spectra into a CoIA framework. This addresses a long-standing gap in core analysis: the lack of a quantitative method capable of simultaneously characterizing both dimensions within a unified analytical framework. In both assemblages neither the global Mantel test nor the RV coefficient reached significance, and the CoIA line-direction analyses revealed no structured techno-morphological covariation within core types.

This analytical result has both theoretical and methodological implications. In terms of theories of core exploitation, the absence of detectable covariation suggests that core morphology and reduction strategy respond to different constraints and should not be treated as interchangeable proxies for one another in archaeological interpretation. This does not imply that conventional core typologies are invalid. Rather, it suggests that their coherence depends on dimensions beyond global morphology and global scar organization, including locally expressed technological features such as flaking angle, platform preparation, and the organization of specific flaking surfaces. The relationship between technological intention and core form may therefore be better addressed through these more localized and technologically diagnostic variables than through overall core morphology alone. Methodologically, it supports the analytical approach adopted here, in which morphology and scar pattern are characterized as separate yet complementary dimensions rather than collapsed into a single typological classification. The CoIA framework, combined with the reconstructive capacity of spherical harmonics, further enables this variation to be visualized as continuous trajectories along covariance gradients rather than as discrete typological categories, moving beyond static classification toward a dynamic representation of techno-morphological variability. As an exploratory tool, CoIA remains informative even under decoupling, since it characterizes the overall structure of variation within an assemblage. Where sample sizes permit, a more powerful application would be to run it separately within each core type, capturing the within-type spectrum of techno-morphological variation that our present per-type samples are too small to resolve. This decoupling is robust to analytical choices: across all vMF kernel bandwidths, scar size thresholds, and mesh preprocessing settings tested, the morphology–scar pattern association remained negligible in magnitude (Mantel's $r \approx 0$; $RV \approx 0.06$–0.12 across both assemblages; Online Resource 1). RV crossed the 0.05 threshold only under the two most extreme settings (an over-smoothed kernel and an unsmoothed mesh), where it remained negligible and was uncorroborated by the Mantel test. A complementary power analysis further suggests that this pattern is unlikely to reflect limited sample size alone, since moderate associations would probably have been detected (Online Resource 1).

Our application of the framework to the SDG assemblage provides a direct test of its performance on archaeological materials while yielding new behavioral insights. Previous studies proposed that lithic technology at SDG remained broadly continuous across layers, with two principal operational sequences: a small-flake system based on chert and a large-flake and LCT system based on quartz sandstone (H. Li *et al.*, 2022). However, whether these two raw material systems involve distinct reduction strategies at a finer behavioral level has not been fully explored. The present results provide quantitative support for technological continuity: no significant differences in either core morphology or scar pattern were detected between Layers 4 and 3, confirming that reduction behavior remained stable across the stratigraphic sequence.

At the same time, the framework clarifies the relative roles of the factors structuring core variation at SDG. Core type was the dominant influence on both morphology and scar organization, explaining several times more variation than raw material or stratigraphic layer. Raw material had only a small, non-significant effect on morphology and a negligible effect on scar organization, while layer effects were negligible throughout. Reduction intensity, which is often closely associated with changes in core morphology and technological organization (Lombao *et al.*, 2023a, 2023b), likewise did not structure either dimension in any detectable way, whether considered overall or separately by raw material and layer. This suggests that differences in form and scar organization derive more from the reduction strategies themselves than from where each core sits along its reduction. This pattern indicates that knapping behavior at SDG was structured primarily by the kind of core being produced rather than by raw material, by time, or by reduction stage, consistent with a stable technological tradition. The decoupling of the two dimensions held consistently across the assemblage: no core type, raw material, or stratigraphic layer exhibited a distinct structured techno-morphological trajectory. However, the present design can only exclude effects of moderate size, and the per-type sample sizes are too small to test whether individual core types follow their own trajectories. The sample size at Sandinggai is relatively limited, with fewer than ten specimens represented in some core types under the current classification scheme. Therefore, this case study is intended primarily to demonstrate what the framework can and cannot resolve from archaeological material, rather than to provide a comprehensive technological analysis of the site. More broadly, the capacity to attribute variation to these competing factors, and to show that morphology and scar organization respond to them largely independently, would be difficult to achieve without the separate quantification of both dimensions afforded by our framework. Wherever assemblages combine multiple raw materials, the same approach can investigate whether material differences are expressed in form, in reduction organization, or in both.

From a broader perspective, the framework proposed here offers potential analytical pathways for addressing several unresolved issues in current studies, none of which the present case study speaks to directly. For example, the presence of Levallois technology in China has been a matter of persistent contention, with ongoing disagreements over whether specific cores from sites such as Guanyindong and Shiyu fulfill Levallois criteria (Carmignani *et al.*, 2024; Hu *et al.*, 2019, 2023; F. Li *et al.*, 2019; Yang *et al.*, 2024a, 2024b). The SPHARM framework, by providing continuous quantitative descriptors independent of subjective typological boundaries, may offer additional analytical perspectives for such debates. Similarly, the evolutionary relationship between Levallois technology and Acheulean industries remains a central question in Lower–Middle Paleolithic transition research globally. Competing hypotheses include independent invention, derivation from handaxe traditions, and development from earlier prepared-core technologies (Adler *et al.*, 2014; Agam *et al.*, 2022; Moncel *et al.*, 2020; Rosenberg-Yefet *et al.*, 2021; Shipton *et al.*, 2013). Recent landmark-based geometric morphometric studies have compared Levallois cores, simple prepared cores, and handaxes, suggesting multiple regional trajectories of origin (Gill *et al.*, 2025). However, landmark configurations may vary between researchers, limiting cross-study integration and large-scale comparative potential (Bardua *et al.*, 2019; Collyer *et al.*, 2020; Webster & Sheets, 2010). This is not to understate the strengths of the approach: sliding semilandmarks minimize bending energy to improve correspondence across specimens, which enhances comparability and often increases discriminatory power (Bardua *et al.*, 2019; Gunz & Mitteroecker, 2013). Rather than replacing landmark-based approaches, SPHARM is complementary to them (Harper *et al.*, 2022): because it does not rely on homologous landmarks and produces standardized spectral descriptors, it is particularly suited to comparisons across core types, assemblages and periods, where landmark homology is hardest to establish. Although the current application focuses on cores and does not yet include large cutting tools, the method is in principle applicable to such types. To support the adoption of this framework, we provide an open-source R package (spharmlithic) that implements the main analytical methods developed in this study, including model alignment, SPI and fabric computation, spherical harmonic analysis of both scar patterns and core morphology, and three-dimensional visual reconstruction (Xiao & Marwick, 2026). The package is accompanied by vignettes documenting each function and providing a worked example of the complete workflow, from model alignment through to the joint analysis, allowing students and researchers to easily and freely apply the methods developed here to their own datasets without requiring specialist programming expertise.

More broadly, the approach has potential for integration with emerging analytical paradigms. Recent work has incorporated elliptic Fourier series into phylogenetic analyses, though these applications have been restricted to two-dimensional morphologies of flaking products (Matzig *et al.*, 2024). As a three-dimensional generalization of Fourier methods, spherical harmonic analysis could be extended to phylogenetic frameworks. The scar pattern component developed here is particularly relevant in this regard, as it provides a direct line of evidence for reconstructing reduction strategies. Future integration with phylogenetic modeling may offer new opportunities to investigate technological transmission and processes of social learning among hominin groups.

Several limitations should be acknowledged. First, sample sizes for certain core types, particularly bidirectional and discoidal cores in the experimental assemblage, are small, and the current results should therefore be interpreted as exploratory rather than definitive. Second, the experimental cores were produced by a single knapper, which may not fully capture the range of inter-individual variability expected in archaeological assemblages. The scar vectors were also recorded by a single analyst. While the perturbation analysis quantifies how the descriptors respond to annotation error of a given magnitude (Online Resource 1), establishing the actual error rate would require independent annotation of the same specimens by multiple analysts, as recently undertaken for scar chronology (Kot *et al.*, 2025; Liu *et al.*, 2026). Third, scar chronology constitutes a further dimension of scar evidence that the present framework does not address. Recent work has quantified the error rate of manual chronological determination (Kot *et al.*, 2025) and has begun to approach the problem computationally from 3D models (Linsel *et al.*, 2025; Liu *et al.*, 2026). Integrating orientation-based and sequence-based descriptors is a promising direction for future work. Finally, the present study operates at the core level, characterizing overall morphology and scar organization as aggregate properties. Finer-grained technological attributes, such as platform preparation and flaking surface maintenance, are not captured by the current framework. Future study should combine quantitative analyses across multiple scales, progressing from macroscopic to microscopic levels in order to comprehensively characterize lithic variability and more clearly elucidate hominin technological strategies.

Conclusion

This study introduces a spherical harmonic framework for the integrated three-dimensional analysis of lithic cores, extending SPHARM beyond near-spherical artifacts to a broader range of morphologically diverse core types. The framework characterizes core morphology (M-SPHARM) and scar pattern (SP-SPHARM) within the same mathematical representation, using von Mises–Fisher kernel density estimation to convert discrete scar vectors into continuous spherical distributions amenable to harmonic expansion.

Validation against idealized digital cores and experimentally knapped cores demonstrates that SP-SPHARM resolves finer distinctions than existing approaches, most notably separating radial core subtypes such as Levallois and discoidal that neither SPI nor fabric metrics can resolve. The three methods nonetheless capture different aspects of scar organization and are best used in combination: SP-SPHARM for overall structural comparison, SPI and fabric metrics for interpretively grounded refinement.

Building on these descriptors, we further introduce a co-inertia analysis framework as a companion approach for jointly examining technological and morphological variation. Applied to experimental and archaeological assemblages, this exploratory framework reveals no detectable covariation between core morphology and scar organization at the assemblage level, a decoupling that holds broadly across core types, raw materials, and stratigraphic layers. These findings should be regarded as preliminary, but they illustrate the analytical possibilities opened up by treating morphology and scar pattern as separate yet jointly analyzable dimensions.

Finally, in support of broader adoption of our framework, we offer spharmlithic, an open-source R package including walk-through documentation. This conveniently implements the essential analytical methods developed in this study, including model alignment, SPI and fabric computation, SPHARM analysis of both morphology and scar patterns, and three-dimensional visual reconstruction. The package, together with the version-controlled repository containing the complete analysis scripts and data for this paper, enables both independent reproduction of the reported results and application of the methods to new datasets.

Future work should focus on expanding sample sizes and assemblage diversity and integrating SPHARM with phylogenetic and other emerging quantitative paradigms to investigate broader questions of the technological behavior of past humans.

Supplementary Information The online version contains supplementary material available at https://doi.org/10.1007/s10816-026-09828-7.

Acknowledgements We are grateful to Chris Clarkson of Griffith University and Sam Lin of the University of Wollongong for generously sharing the idealized digital core dataset and the experimentally knapped core dataset, and for permitting us to make this high-quality dataset publicly available. We also thank Yiyuan Li of the Hunan Provincial Institute of Cultural Relics and Archaeology for providing access to the Sandinggai specimens for this study.

Author Contribution P. X.: conceptualization, data curation, formal analysis, investigation, methodology, software, validation, visualization, and writing—original draft; H. L.: funding acquisition, resources, supervision, and writing—review and editing; B. M.: conceptualization, methodology, software, supervision, validation, and writing—review and editing. All authors reviewed and approved the final manuscript.

Funding This work was financially supported by the Archaeological Talent Promotion Program of China (No. 2025–198, to H.L.), the National Natural Science Foundation of China (Nos. U2574202 and 42471180, to H.L.), and the China Scholarship Council Program for International Students (CSC No. 202504910326, to P.X.).

Data Availability All data and code required to reproduce this study, including the 3D core models, scar orientation and observational data, and the complete R and Python analysis code, are archived in the project's OSF repository (https://doi.org/10.17605/OSF.IO/D82C5). The repository includes a README file that describes its structure in detail and provides step-by-step instructions for reproducing the analyses.

Declarations

Competing Interests The authors declare no competing interests.

References

Adler, D. S., Wilkinson, K. N., Blockley, S., Mark, D. F., Pinhasi, R., Schmidt-Magee, B. A., *et al.* (2014). Early Levallois technology and the Lower to Middle Paleolithic transition in the Southern Caucasus. *Science, 345*(6204), 1609–1613. https://doi.org/10.1126/science.1256484

Agam, A., Rosenberg-Yefet, T., Wilson, L., Shemer, M., & Barkai, R. (2022). Flint type analysis at late Acheulian Jaljulia (Israel), and implications for the origins of prepared core technologies. *Frontiers in Earth Science, 10*,. https://doi.org/10.3389/feart.2022.858032

Aitchison, J. (1982). The statistical analysis of compositional data. *Journal of the Royal Statistical Society. Series B, Statistical Methodology, 44*(2), 139–160. https://doi.org/10.1111/j.2517-6161.1982.tb01195.x

Alonso-Pena, M., Claeskens, G., & Gijbels, I. (2024). Nonparametric estimation of densities on the hypersphere using a parametric guide. *Scandinavian Journal of Statistics, 51*(3), 956–986. https://doi.org/10.1111/sjos.12737

Anderson, M. J. (2001). A new method for non-parametric multivariate analysis of variance. *Austral Ecology, 26*(1), 32–46. https://doi.org/10.1111/j.1442-9993.2001.01070.pp.x

Anderson, M. J. (2006). Distance-based tests for homogeneity of multivariate dispersions. *Biometrics, 62*(1), 245–253. https://doi.org/10.1111/j.1541-0420.2005.00440.x

Anderson, M. J. (2017). Permutational multivariate analysis of variance (PERMANOVA). In R. S. Kenett, N. T. Longford, W. W. Piegorsch, & F. Ruggeri (Eds.), *Wiley statsref: Statistics reference online* (1st ed., pp. 1–15). Wiley. https://doi.org/10.1002/9781118445112.stat07841

Archer, W., Djakovic, I., Brenet, M., Bourguignon, L., Presnyakova, D., Schlager, S., *et al.* (2021). Quantifying differences in hominin flaking technologies with 3D shape analysis. *Journal of Human Evolution, 150*,. https://doi.org/10.1016/j.jhevol.2020.102912

Arnold, B. C., & SenGupta, A. (2006). Probability distributions and statistical inference for axial data. *Environmental and Ecological Statistics, 13*(3), 271–285. https://doi.org/10.1007/s10651-004-0011-8

Bai, Z. D., Rao, C. R., & Zhao, L. C. (1988). Kernel estimators of density function of directional data. *Journal of Multivariate Analysis, 27*(1), 24–39. https://doi.org/10.1016/0047-259X(88)90113-3

Bardua, C., Felice, R. N., Watanabe, A., Fabre, A.-C., & Goswami, A. (2019). A practical guide to sliding and surface semilandmarks in morphometric analyses. *Integrative Organismal Biology, 1*(1). https://doi.org/10.1093/iob/obz016

Benn, D. (1994). Fabric shape and the interpretation of sedimentary fabric data. *Journal of Sedimentary Research, 64*(4a), 910–915. https://doi.org/10.1306/D4267F05-2B26-11D7-8648000102C1865D

Bland, J. M., & Altman, D. G. (1986). Statistical methods for assessing agreement between two methods of clinical measurement. *The Lancet, 327*(8476), 307–310. https://doi.org/10.1016/S0140-6736(86)90837-8

Bland, J. M., & Altman, D. G. (1999). Measuring agreement in method comparison studies. *Statistical Methods in Medical Research, 8*(2), 135–160. https://doi.org/10.1177/096228029900800204

Boëda, E. (1993). Le débitage discoïde et le débitage Levallois récurrent centripède. *Bulletin De La Société Préhistorique Française, 90*(6), 392–404. https://doi.org/10.3406/bspf.1993.9669

Boëda, E. (1995). Levallois: A volumetric construction, methods, a technique. In H. L. Dibble & O. Bar-Yosef (Eds.), *The definition and interpretation of Levallois technology* (pp. 41–68). Prehistory Press.

Brantingham, P. J., & Kuhn, S. L. (2001). Constraints on levallois core technology: A mathematical model. *Journal of Archaeological Science, 28*(7), 747–761. https://doi.org/10.1006/jasc.2000.0594

Brechbühler, C., Gerig, G., & Kübler, O. (1995). Parametrization of closed surfaces for 3-D shape description. *Computer Vision and Image Understanding, 61*(2), 154–170.

Bretzke, K., & Conard, N. J. (2012). Evaluating morphological variability in lithic assemblages using 3D models of stone artifacts. *Journal of Archaeological Science, 39*(12), 3741–3749. https://doi.org/10.1016/j.jas.2012.06.039

Bustos-Pérez, G., Gravina, B., Brenet, M., & Romagnoli, F. (2022). Combining quantitative approaches to differentiate between backed products from discoidal and Levallois reduction sequences. *Journal of Archaeological Science: Reports, 46*,. https://doi.org/10.1016/j.jasrep.2022.103723

Cao, Y., Yi, M., Chen, F., & Wang, H. (2025). Lithic variability and raw material exploitation strategies at Shuidonggou locality 12, China: A quantitative approach. *Archaeometry, 67*(6), 1515–1530. https://doi.org/10.1111/arcm.13106

Carmignani, L., Djakovic, I., Zhang, P., Teyssandier, N., Zwyns, N., & Soressi, M. (2024). An initial Upper Palaeolithic attribution is not empirically supported at Shiyu, northern China. *Nature Ecology & Evolution, 9*(1), 34–37. https://doi.org/10.1038/s41559-024-02548-9

Cattabriga, G., Gramigna, A., & Peresani, M. (2024). Exploring knapping learning processes amongst Upper Palaeolithic hunter-gatherers. *History of Education, 53*(3), 439–459. https://doi.org/10.1080/0046760X.2023.2223545

Cattabriga, G., & Peresani, M. (2024). Criteria for identifying knapping skill level through the analysis of lithic cores: An example from Val Lastari, Late Palaeolithic. *Italy. Lithic Technology, 49*(4), 416–431. https://doi.org/10.1080/01977261.2024.2303230

Clarkson, C. (2013). Measuring core reduction using 3D flake scar density: A test case of changing core reduction at Klasies River Mouth, South Africa. *Journal of Archaeological Science, 40*(12), 4348–4357. https://doi.org/10.1016/j.jas.2013.06.007

Clarkson, C., Vinicius, L., & Lahr, M. M. (2006). Quantifying flake scar patterning on cores using 3D recording techniques. *Journal of Archaeological Science, 33*(1), 132–142. https://doi.org/10.1016/j.jas.2005.07.007

Collyer, M. L., Davis, M. A., & Adams, D. C. (2020). Making heads or tails of combined landmark configurations in geometric morphometric data. *Evolutionary Biology, 47*(3), 193–205. https://doi.org/10.1007/s11692-020-09503-z

Conard, N. J., Soressi, M., Parkington, J. E., Wurz, S., & Yates, R. (2004). A unified lithic taxonomy based on patterns of core reduction. *The South African Archaeological Bulletin, 59*(179), 12. https://doi.org/10.2307/3889318

Delagnes, A., & Meignen, L. (2006). Diversity of lithic production systems during the middle paleolithic in France: Are there any chronological trends? In E. Hovers & S. L. Kuhn (Eds.), *Transitions before the transition: Evolution and stability in the Middle Paleolithic and Middle Stone Age* (pp. 85–107). Springer US. https://doi.org/10.1007/0-387-24661-4_5

Delpiano, D., & Peresani, M. (2017). Exploring Neanderthal skills and lithic economy. The implication of a refitted discoid reduction sequence reconstructed using 3D virtual analysis. *Comptes Rendus Palevol, 16*(8), 865–877. https://doi.org/10.1016/j.crpv.2017.06.008

Dibble, H. L. (1991). Local raw material exploitation and its effects on lower and middle Paleolithic assemblage variability. In A. Montet-White & S. Holen (Eds.), *Raw material economies among prehistoric hunter-gatherers* (pp. 34–47). University of Kansas Publications in Anthropology.

Dolédec, S., & Chessel, D. (1994). Co-inertia analysis: An alternative method for studying species-environment relationships. *Freshwater Biology, 31*(3), 277–294. https://doi.org/10.1111/j.1365-2427.1994.tb01741.x

Douglass, M. J., Lin, S. C., Braun, D. R., & Plummer, T. W. (2018). Core use-life distributions in lithic assemblages as a means for reconstructing behavioral patterns. *Journal of Archaeological Method and Theory, 25*(1), 254–288. https://doi.org/10.1007/s10816-017-9334-2

Dray, S., Chessel, D., & Thioulouse, J. (2003). Co-inertia analysis and the linking of ecological data tables. *Ecology, 84*(11), 3078–3089. https://doi.org/10.1890/03-0178

Egozcue, J. J., Pawlowsky-Glahn, V., Mateu-Figueras, G., & Barceló-Vidal, C. (2003). Isometric log ratio transformations for compositional data analysis. *Mathematical Geology, 35*(3), 279–300. https://doi.org/10.1023/A:1023818214614

Eren, M. I., Bradley, B. A., & Sampson, C. G. (2011). Middle Paleolithic skill level and the individual knapper: An experiment. *American Antiquity, 76*(2), 229–251. https://doi.org/10.7183/0002-7316.76.2.229

Escoufier, Y. (1973). *Le Traitement des Variables Vectorielles. Biometrics, 29*(4), 751. https://doi.org/10.2307/2529140

Falcucci, A., & Peresani, M. (2022). The contribution of integrated 3D model analysis to Protoaurignacian stone tool design. *PLoS ONE, 17*(5). https://doi.org/10.1371/journal.pone.0268539

Gerig, G., Styner, M., Jones, D., Weinberger, D., & Lieberman, J. (2001). Shape analysis of brain ventricles using SPHARM. In *Proceedings of the IEEE workshop on mathematical methods in biomedical image analysis* (pp. 171–178). Kauai, HI, USA: IEEE Computer Society. https://doi.org/10.1109/MMBIA.2001.991731

Gill, J. P., Ashton, N., Wilkinson, K. N., Gasparyan, B., & Adler, D. S. (2025). The shape of technology to come: An examination of evolutionary relationships between bifacial and core technologies at the Lower-Middle Palaeolithic boundary across regions in Eurasia. *Journal of Human Evolution, 205*,. https://doi.org/10.1016/j.jhevol.2025.103702

Goldberg, D. (1991). What every computer scientist should know about floating-point arithmetic. *ACM Computing Surveys, 23*(1), 5–48. https://doi.org/10.1145/103162.103163

Goswami, A., Watanabe, A., Felice, R. N., Bardua, C., Fabre, A.-C., & Polly, P. D. (2019). High-density morphometric analysis of shape and integration: The good, the bad, and the not-really-a-problem. *Integrative and Comparative Biology, 59*(3), 669–683. https://doi.org/10.1093/icb/icz120

Greenacre, M. (2021). Compositional data analysis. *Annual Review of Statistics and Its Application, 8*, 271–299. https://doi.org/10.1146/annurev-statistics-042720-124436

Grosman, L., Smikt, O., & Smilansky, U. (2008). On the application of 3-D scanning technology for the documentation and typology of lithic artifacts. *Journal of Archaeological Science, 35*(12), 3101–3110. https://doi.org/10.1016/j.jas.2008.06.011

Gunz, P., & Mitteroecker, P. (2013). Semilandmarks: A method for quantifying curves and surfaces. *Hystrix, the Italian Journal of Mammalogy*. https://doi.org/10.4404/hystrix-24.1-6292

Hallinan, E., & Cascalheira, J. (2025). Quantifying Levallois: A 3D geometric morphometric approach to Nubian technology. *Archaeological and Anthropological Sciences, 17*(4), 88. https://doi.org/10.1007/s12520-025-02199-2

Hallinan, E., Shaw, M., Shaw, C., & Samawi, O. (2026). The Nubian spectrum: 3D geometric morphometric perspectives on Levallois core reduction at Tweefontein. *South Africa. Journal of Paleolithic Archaeology, 9*(1), 10. https://doi.org/10.1007/s41982-025-00244-z

Hamby, D. M. (1994). A review of techniques for parameter sensitivity analysis of environmental models. *Environmental Monitoring and Assessment, 32*(2), 135–154. https://doi.org/10.1007/BF00547132

Harper, C. M., Goldstein, D. M., & Sylvester, A. D. (2022). Comparing and combining sliding semilandmarks and weighted spherical harmonics for shape analysis. *Journal of Anatomy, 240*(4), 678–687. https://doi.org/10.1111/joa.13589

Hashemi, S. M., VahdatiNasab, H., Berillon, G., & Oryat, M. (2021). An investigation of the flake-based lithic tool morphology using 3D geometric morphometrics: A case study from the Mirak Paleolithic Site. *Iran. Journal of Archaeological Science: Reports, 37*,. https://doi.org/10.1016/j.jasrep.2021.102948

Herzlinger, G., Goren-Inbar, N., & Grosman, L. (2017). A new method for 3D geometric morphometric shape analysis: The case study of handaxe knapping skill. *Journal of Archaeological Science: Reports, 14*, 163–173. https://doi.org/10.1016/j.jasrep.2017.05.013

Higham, N. J. (2002). *Accuracy and stability of numerical algorithms* (2nd ed.). SIAM. https://doi.org/10.1137/1.9780898718027

Hoenig, J. M., & Heisey, D. M. (2001). The abuse of power: The pervasive fallacy of power calculations for data analysis. *The American Statistician, 55*(1), 19–24. https://doi.org/10.1198/000313001300339897

Holm, S. (1979). A simple sequentially rejective multiple test procedure. *Scandinavian Journal of Statistics, 6*(2), 65–70.

Hu, Y., Marwick, B., Lu, H., Hou, Y., Huang, W., & Li, B. (2023). Evidence of Levallois strategies on cores at Guanyindong cave, Southwest China during the late middle Pleistocene. *Journal of Archaeological Science: Reports, 47*,. https://doi.org/10.1016/j.jasrep.2022.103727

Hu, Y., Marwick, B., Zhang, J.-F., Rui, X., Hou, Y.-M., Yue, J.-P., *et al.* (2019). Late middle Pleistocene Levallois stone-tool technology in southwest China. *Nature, 565*(7737), 82–85. https://doi.org/10.1038/s41586-018-0710-1

Hutton, T. J., Buxton, B. F., Hammond, P., & Potts, H. W. W. (2003). Estimating average growth trajectories in shape-space using kernel smoothing. *IEEE Transactions on Medical Imaging, 22*(6), 747–753. https://doi.org/10.1109/TMI.2003.814784

Inizan, M.-L., & Féblot-Augustins, J. (Eds.). (1999). *Technology and terminology of knapped stone: Followed by a multilingual vocabulary - Arabic, English, French, German, Greek, Italian, Portuguese, Spanish*. Cercle de Recherches et d'Etudes Préhistoriques (CNRS), Meudon.

Kazhdan, M., Funkhouser, T., & Rusinkiewicz, S. (2003). Rotation invariant spherical harmonic representation of 3D shape descriptors. In *Proceedings of the 2003 Eurographics/ACM SIGGRAPH Symposium on Geometry Processing* (pp. 156–164). Eurographics Association. https://doi.org/10.2312/SGP/SGP03/156-164

Kot, M., Pavlenok, K., Krajcarz, M. T., Pavlenok, G., Shnaider, S., Khudjanazarov, M., *et al.* (2020). Raw material procurement as a crucial factor determining knapping technology in the Katta Sai complex of Middle Palaeolithic sites in the western Tian Shan piedmonts of Uzbekistan. *Quaternary International, 559*, 97–109. https://doi.org/10.1016/j.quaint.2020.03.052

Kot, M., Tyszkiewicz, J., Leloch, M., Gryczewska, N., & Miller, S. (2025). Reliability and validity in determining the relative chronology between neighbouring scars on flint artefacts. *Journal of Archaeological Science, 175*,. https://doi.org/10.1016/j.jas.2025.106156

Kruskal, W. H., & Wallis, W. A. (1952). Use of ranks in one-criterion variance analysis. *Journal of the American Statistical Association, 47*(260), 583–621. https://doi.org/10.1080/01621459.1952.10483441

Lakens, D. (2022). Sample size justification. *Collabra: Psychology, 8*(1). https://doi.org/10.1525/collabra.33267

Lee, K. J., Danhaive, R., & Mueller, C. T. (2022). Spherical harmonic shape descriptors of nodal force demands for quantifying spatial truss connection complexity. *Architecture, Structures and Construction, 2*(1), 145–164.

Li, F., Li, Y., Gao, X., L Kuhn, S., Boëda, E., & W Olsen, J. (2019). A refutation of reported Levallois technology from Guanyindong cave in south China. *National Science Review, 6*(6), 1094–1096. https://doi.org/10.1093/nsr/nwz115

Li, H., Kuman, K., Lotter, M. G., Leader, G. M., & Gibbon, R. J. (2017). The Victoria West: Earliest prepared core technology in the Acheulean at Canteen Kopje and implications for the cognitive evolution of early hominids. *Royal Society Open Science, 4*(6), 170–288. https://doi.org/10.1098/rsos.170288

Li, H., Lei, L., Li, D., Lotter, M. G., & Kuman, K. (2021). Characterizing the shape of large cutting tools from the Baise Basin (South China) using a 3D geometric morphometric approach. *Journal of Archaeological Science: Reports, 36*,. https://doi.org/10.1016/j.jasrep.2021.102820

Li, H., Li, Y., Yu, L., Tu, H., Zhang, Y., Sumner, A., & Kuman, K. (2022). Continuous technological and behavioral development of late Pleistocene hominins in central South China: Multidisciplinary analysis at Sandinggai. *Quaternary Science Reviews, 298*,. https://doi.org/10.1016/j.quascirev.2022.107850

Lin, S. C., Clarkson, C., Julianto, I. M. A., Ferdianto, A., Jatmiko, & Sutikna, T. (2024). A new method for quantifying flake scar organisation on cores using orientation statistics. *Journal of Archaeological Science*, *167*, 105998. https://doi.org/10.1016/j.jas.2024.105998

Lin, S. C., Douglass, M. J., Holdaway, S. J., & Floyd, B. (2010). The application of 3D laser scanning technology to the assessment of ordinal and mechanical cortex quantification in lithic analysis. *Journal of Archaeological Science, 37*(4), 694–702. https://doi.org/10.1016/j.jas.2009.10.030

Linsel, F., Bullenkamp, J. P., & Mara, H. (2025). From scar to scar: Reconstructing operational sequences of lithic artifacts using scar-ridge-pattern-based graph models. *Computer Applications and Quantitative Methods in Archaeology Proceedings, 51*(1), 1. https://doi.org/10.64888/caaproceedings.v51i1.725

Liu, C., Valletta, F., BaenaPreysler, J., & Falcucci, A. (2026). Reconstructing the sequentiality of adjacent flake removal scars on lithic 3D models: A curvature-based computational approach. *Archaeological and Anthropological Sciences, 18*(6), 150. https://doi.org/10.1007/s12520-026-02510-9

Lombao, D., Cueva-Temprana, A., Mosquera, M., & Morales, J. I. (2020). A new approach to measure reduction intensity on cores and tools on cobbles: The volumetric reconstruction method. *Archaeological and Anthropological Sciences, 12*(9), 222. https://doi.org/10.1007/s12520-020-01154-7

Lombao, D., Falcucci, A., Moos, E., & Peresani, M. (2023). Unravelling technological behaviors through core reduction intensity. The case of the early Protoaurignacian assemblage from Fumane Cave. *Journal of Archaeological Science, 160*,. https://doi.org/10.1016/j.jas.2023.105889

Lombao, D., Morales, J. I., Mosquera, M., Ollé, A., Saladié, P., & Vallverdú, J. (2024). Beyond large-shaped tools: Technological innovations and continuities at the late early pleistocene assemblage of el barranc de la boella (tarragona, spain). *Journal of Paleolithic Archaeology, 7*(1), 25. https://doi.org/10.1007/s41982-024-00189-9

Lombao, D., Rabuñal, J. R., Morales, J. I., Ollé, A., Carbonell, E., & Mosquera, M. (2023). The technological behaviours of *Homo antecessor*: Core management and reduction intensity at Gran Dolina-TD6.2 (Atapuerca, Spain). *Journal of Archaeological Method and Theory, 30*(3), 964–1001. https://doi.org/10.1007/s10816-022-09579-1

Lycett, S. J., Cramon-Taubadel, N. V., & Gowlett, J. A. J. (2010). A comparative 3D geometric morphometric analysis of Victoria West cores: Implications for the origins of Levallois technology. *Journal of Archaeological Science, 37*(5), 1110–1117. https://doi.org/10.1016/j.jas.2009.12.011

Lycett, S. J., & Von Cramon-Taubadel, N. (2013). A 3D morphometric analysis of surface geometry in Levallois cores: Patterns of stability and variability across regions and their implications. *Journal of Archaeological Science, 40*(3), 1508–1517. https://doi.org/10.1016/j.jas.2012.11.005

Mantel, N. (1967). The detection of disease clustering and a generalized regression approach. *Cancer Research, 27*(2), 209–220.

Mardia, K. V. (1988). Directional data analysis: An overview. *Journal of Applied Statistics, 15*(2), 115–122. https://doi.org/10.1080/02664768800000018

Mark, D. M. (1973). Analysis of axial orientation data, including till fabrics. *Geological Society of America Bulletin, 84*(4), 1369. https://doi.org/10.1130/0016-7606(1973)84%3c1369:AOAODI>2.0.CO;2

Marwick, B. (2017). Computational reproducibility in archaeological research: Basic principles and a case study of their implementation. *Journal of Archaeological Method and Theory, 24*(2), 424–450. https://doi.org/10.1007/s10816-015-9272-9

Marwick, B., Guedes, J. d'Alpoim, Barton, C. M., Bates, L. A., Baxter, M., Bevan, A., *et al*. (2017). Open science in archaeology. *SAA Archaeological Record*, *17*(4), 8–14. https://doi.org/10.31235/osf.io/72n8g

Matzig, D. N., Marwick, B., Riede, F., & Warnock, R. C. M. (2024). A macroevolutionary analysis of European Late Upper Palaeolithic stone tool shape using a Bayesian phylodynamic framework. *Royal Society Open Science, 11*(8). https://doi.org/10.1098/rsos.240321

McPherron, S. P. (2018). Additional statistical and graphical methods for analyzing site formation processes using artifact orientations. *PLoS ONE, 13*(1). https://doi.org/10.1371/journal.pone.0190195

Medyukhina, A., Blickensdorf, M., Cseresnyés, Z., Ruef, N., Stein, J. V., & Figge, M. T. (2020). Dynamic spherical harmonics approach for shape classification of migrating cells. *Scientific Reports, 10*(1), 6072. https://doi.org/10.1038/s41598-020-62997-7

Moncel, M.-H., Ashton, N., Arzarello, M., Fontana, F., Lamotte, A., Scott, B., *et al.* (2020). Early Levallois core technology between marine isotope stage 12 and 9 in Western Europe. *Journal of Human Evolution, 139*,. https://doi.org/10.1016/j.jhevol.2019.102735

Muller, A., Barsky, D., Sala-Ramos, R., Sharon, G., Titton, S., Vergès, J.-M., & Grosman, L. (2023). The limestone spheroids of 'Ubeidiya: Intentional imposition of symmetric geometry by early hominins? *Royal Society Open Science, 10*(9). https://doi.org/10.1098/rsos.230671

Muller, A., & Clarkson, C. (2026). Getting into shape: Computing continua of Middle Stone Age prepared core technology. *World Archaeology*. https://doi.org/10.1080/00438243.2026.2641452

Muller, A., Shipton, C., & Clarkson, C. (2022). Stone toolmaking difficulty and the evolution of hominin technological skills. *Scientific Reports, 12*(1), 5883. https://doi.org/10.1038/s41598-022-09914-2

Pandey, A. (2025). A study of lithic refitting and the Middle Palaeolithic core reduction strategies in South Bihar. *India. Archaeological and Anthropological Sciences, 17*(7), 155. https://doi.org/10.1007/s12520-025-02261-z

Pargeter, J., Brooks, A., Douze, K., Eren, M., Groucutt, H. S., McNeil, J., *et al.* (2023). Replicability in lithic analysis. *American Antiquity, 88*(2), 163–186. https://doi.org/10.1017/aaq.2023.4

Pargeter, J., Liu, C., Kilgore, M. B., Majoe, A., & Stout, D. (2022). Testing the effect of learning conditions and individual motor/cognitive differences on knapping skill acquisition. *Journal of Archaeological Method and Theory, 30*, 127–171. https://doi.org/10.1007/s10816-022-09592-4

Porter, S. T., Roussel, M., & Soressi, M. (2019). A comparison of Châtelperronian and Protoaurignacian core technology using data derived from 3D models. *Journal of Computer Applications in Archaeology, 2*(1), 41–55. https://doi.org/10.5334/jcaa.17

Proffitt, T., Bargalló, A., & De La Torre, I. (2022). The effect of raw material on the identification of knapping skill: A case study from Olduvai Gorge, Tanzania. *Journal of Archaeological Method and Theory, 29*(1), 50–82. https://doi.org/10.1007/s10816-021-09511-z

Radvilaitė, U., Ramírez-Gómez, Á., & Kačianauskas, R. (2016). Determining the shape of agricultural materials using spherical harmonics. *Computers and Electronics in Agriculture, 128*, 160–171. https://doi.org/10.1016/j.compag.2016.09.003

Robert, P., & Escoufier, Y. (1976). A unifying tool for linear multivariate statistical methods: The RV-coefficient. *Applied Statistics, 25*(3), 257. https://doi.org/10.2307/2347233

Rohlf, F. J., & Corti, M. (2000). Use of two-block partial least-squares to study covariation in shape. *Systematic Biology, 49*(4), 740–753. https://doi.org/10.1080/106351500750049806

Rosenberg-Yefet, T., Shemer, M., & Barkai, R. (2021). Acheulian shortcuts: Cumulative culture and the use of handaxes as cores for the production of predetermined blanks. *Journal of Archaeological Science: Reports, 36*,. https://doi.org/10.1016/j.jasrep.2021.102822

Ruck, L., Holden, C., Putt, S. S. J., Schick, K., & Toth, N. (2020). Inter- and intra-rater reliability in lithic analysis: A case study in handedness determination methodologies. *Journal of Archaeological Method and Theory, 27*(2), 220–244. https://doi.org/10.1007/s10816-019-09424-y

Saltelli, A. (2002). Sensitivity analysis for importance assessment. *Risk Analysis, 22*(3), 579–590. https://doi.org/10.1111/0272-4332.00040

Shen, L., Farid, H., & McPeek, M. A. (2009). Modeling three-dimensional morphological structures using spherical harmonics. *Evolution, 63*(4), 1003–1016. https://doi.org/10.1111/j.1558-5646.2008.00557.x

Shipton, C., Clarkson, C., Pal, J. N., Jones, S. C., Roberts, R. G., Harris, C., *et al.* (2013). Generativity, hierarchical action and recursion in the technology of the Acheulean to Middle Palaeolithic transition: A perspective from Patpara, the Son Valley, India. *Journal of Human Evolution, 65*(2), 93–108. https://doi.org/10.1016/j.jhevol.2013.03.007

Sholts, S. B., Gingerich, J. A. M., Schlager, S., Stanford, D. J., & Wärmländer, S. K. T. S. (2017). Tracing social interactions in Pleistocene North America via 3D model analysis of stone tool asymmetry. *PLoS ONE, 12*(7). https://doi.org/10.1371/journal.pone.0179933

Terradillos-Bernal, M., & Rodríguez-Álvarez, X.-P. (2014). The influence of raw material qualities in the lithic technology of Gran Dolina (units TD6 and TD10) and Galería (Sierra de Atapuerca, Burgos, Spain): A view from experimental archeology. *Comptes Rendus Palevol, 13*(6), 527–542. https://doi.org/10.1016/j.crpv.2014.02.002

Valletta, F., Dag, I., & Grosman, L. (2021). Identifying local learning communities during the terminal Palaeolithic in the Southern Levant: Multi-scale 3-D analysis of flint cores. *Journal of Computer Applications in Archaeology, 4*(1), 145–168. https://doi.org/10.5334/jcaa.74

Wallace, I. J., & Shea, J. J. (2006). Mobility patterns and core technologies in the Middle Paleolithic of the Levant. *Journal of Archaeological Science, 33*(9), 1293–1309. https://doi.org/10.1016/j.jas.2006.01.005

Wasserstein, R. L., & Lazar, N. A. (2016). The ASA's statement on p-values: Context, process, and purpose. *The American Statistician, 70*(2), 129–133. https://doi.org/10.1080/00031305.2016.1154108

Webster, M., & Sheets, H. D. (2010). A practical introduction to landmark-based geometric morphometrics. *The Paleontological Society Papers, 16*, 163–188. https://doi.org/10.1017/S1089332600001868

Whittaker, J. C., Caulkins, D., & Kamp, K. A. (1998). Evaluating consistency in typology and classification. *Journal of Archaeological Method and Theory, 5*(2), 129–164. https://doi.org/10.1007/BF02427967

Wilson, E. P., Stout, D., Liu, C., Kilgore, M. B., & Pargeter, J. (2023). Skill and core uniformity: An experiment with Oldowan-like flaking systems. *Lithic Technology, 48*(4), 333–346. https://doi.org/10.1080/01977261.2023.2178767

Wyatt-Spratt, S. (2022). After the revolution: A review of 3D modelling as a tool for stone artefact analysis. *Journal of Computer Applications in Archaeology, 5*(1), 215. https://doi.org/10.5334/jcaa.103

Xiao, P., & Marwick, B. (2026). *spharmlithic: Spherical harmonic analysis of lithic morphology and flaking scar patterns*. https://github.com/PeiyuanXiao/spharmlithic. Accessed 28 Aug 2026.

Yang, S.-X., Zhang, J.-F., Yue, J.-P., Huan, F.-X., Ollé, A., d'Errico, F., & Petraglia, M. (2024a). Reply to: An initial Upper Palaeolithic attribution is not empirically supported at Shiyu, northern China. *Nature Ecology & Evolution, 9*(1), 38–41. https://doi.org/10.1038/s41559-024-02554-x

Yang, S.-X., Zhang, J.-F., Yue, J.-P., Wood, R., Guo, Y.-J., Wang, H., *et al.* (2024b). Initial Upper Palaeolithic material culture by 45,000 years ago at Shiyu in northern China. *Nature Ecology & Evolution, 8*(3), 552–563. https://doi.org/10.1038/s41559-023-02294-4

Ye, Z., Pei, S., Ma, D., Li, H., & Marwick, B. (2026). Spherical harmonic analysis of faceted spheroids identifies shaping strategies and standardisation at Qianshangying (North China). *Journal of Archaeological Science, 190*,. https://doi.org/10.1016/j.jas.2026.106551

Zelditch, M. (Ed.). (2004). *Geometric morphometrics for biologists: A primer*. Elsevier Academic Press.

Publisher's Note Springer Nature remains neutral with regard to jurisdictional claims in published maps and institutional affiliations.

Springer Nature or its licensor (e.g. a society or other partner) holds exclusive rights to this article under a publishing agreement with the author(s) or other rightsholder(s); author self-archiving of the accepted manuscript version of this article is solely governed by the terms of such publishing agreement and applicable law.

Authors and Affiliations

Pei-Yuan Xiao[1,2,3] · Hao Li[1,4] · Ben Marwick[3]

✉ Hao Li
lihao@itpcas.ac.cn

✉ Ben Marwick
bmarwick@uw.edu

1 Alpine Paleoecology and Human Adaptation Group (ALPHA Group), State Key Laboratory of Tibetan Plateau Earth System, Environment and Resources, Institute of Tibetan Plateau Research, Chinese Academy of Sciences, Beijing, China

2 University of Chinese Academy of Sciences, Beijing, China

3 Department of Anthropology, University of Washington, Seattle, WA, USA

4 MOE Key Laboratory of Western China's Environmental System, Center for Excellence in Archaeological Science and Cultural Heritage, Lanzhou University, Lanzhou, China